Experimental and Theoretical Studies of the Reaction of the OH Radical with Alkyl Sulfides: 1. Direct Observations of the Formation of the OH−DMS Adduct−Pressure Dependence of the Forward Rate of Addition and Development of a Predictive Expression at Low Temperature

M. B. Williams,[†] P. Campuzano-Jost,[‡] B. M. Cossairt,[§] and A. J. Hynes*

Division of Marine and Atmospheric Chemistry, Rosenstiel School of Marine and Atmospheric Science at the University of Miami, 4600 Rickenbacker Causeway, Miami, Florida 33149

A. J. Pounds

Department of Chemistry, Mercer University, 1400 Coleman Avenue, Macon, Georgia 31207

Received: June 21, 2006; In Final Form: October 26, 2006

A pulsed laser photolysis−pulsed laser-induced fluorescence (PLP-PLIF) system was employed to study the kinetics and mechanisms of reactions (1) OH + h_6-DMS → products and (2) OH + d_6-DMS → products. We report direct observations of the rate coefficients for the formation and dissociation of the h_6-OHDMS and d_6-OHDMS adducts over the pressure range 50−650 Torr and between 240 and 245 K, together with measurements of the oxygen dependence of the effective rate coefficients for reactions 1 and 2 under similar conditions. The effective rate coefficients increased as a function of O_2 concentration reaching their limiting values in each case. The values of the adduct formation rate, obtained from the O_2 dependencies, were in excellent agreement with values determined from direct observation of adduct equilibration in N_2. OH regeneration is insignificant. The rate coefficients for the formation of the adduct isotopomers showed slight differences in their falloff behavior and do not approach the high-pressure limit in either case. The equilibrium constants obtained show no dependence on isotopomer and are in good agreement with previous work. A "second-law" analysis of the temperature dependence of the equilibrium constant gives an adduct bond strength ($\Delta H^o = -10.9 \pm 1.0$ kcal mol^{-1}), also in good agreement with previously reported values. Using the entropy calculated from the ab initio vibrational frequencies, we obtain a "third-law" value for the reaction enthalpy at 240 K, $\Delta H_{240K}{}^o = -10.5$ kcal mol^{-1} in good agreement with the other approach. The rate coefficient for the reactions of the adducts with O_2 was obtained from an analysis of the O_2 dependence and was determined to be $6.3 \pm 1.2 \times 10^{-13}$ cm^3 molecule^{-1} s^{-1}, with no dependence on pressure or isotopomer. The pressure and temperature dependence for all of the elementary processes in the initial steps of the dimethylsulfide (DMS) oxidation mechanism have been characterized in the range 238−245 K, allowing the formulation of an expression which can be used to calculate the effective rate coefficient for reaction 1 at any pressure and oxygen concentration. The expression can calculate the effective rate coefficient for reaction 1 to ±40% over the range 220−260 K, with the largest errors at the extremes of this range. Gaussian 03 has been used to calculate the structure of the OH−DMS adduct and its deuterated isotopomer. We find similar bound structures for both isotopomers. The calculated enthalpies of formation of the adducts are lower than the experimentally determined values.

Introduction

Dimethylsulfide (DMS) is the degradation byproduct of the precursor species dimethyl-sulfonium propionate, DMSP, an osmoregulator found in certain species of phytoplankton.[1] Current estimates of globally averaged DMS emissions are 24.45 ± 5.30 Tg S/yr,[2] composing roughly 16% of global total sulfur emissions and >50% of the Southern Hemisphere's burden.[3] In clean marine air, DMS oxidation is the exclusive source of methane-sulfonic acid (MSA) and is believed to be the dominant source of SO_2.[4] Condensable end products of oxidation, ubiquitous in the marine boundary layer (MBL), can be a significant source of cloud condensation nuclei (CCN),[5] and it has been suggested that DMS could participate in an efficient climate regulating mechanism.[6] Estimates of DMS emissions under future climate scenarios[7−9] suggest the importance of CCN derived from DMS oxidation products will grow for certain regions.

Chemical degradation of DMS in the troposphere involves many kinetic steps with temperature and pressure dependencies suggesting that both the oxidation rate and product distribution will depend on location and the prevailing environmental conditions. The gas-phase oxidation mechanism of DMS has been extensively studied in the laboratory,[10−17] but the quantitative mechanistic details by which particle precursors are formed

* Author to whom correspondence should be addressed.
[†] Current address: Department of Earth System Science, Croul Hall, University of California, Irvine, Irvine, CA 92697.
[‡] Current address: Department of Chemistry, University of British Columbia, Vancouver, British Columbia, CANADA V6T 1Z3.
[§] Current address: Department of Chemistry, Massachusetts Institute of Technology, 77 Massachusetts Ave., Cambridge, MA 02139.

10.1021/jp063873+ CCC: $37.00
Published on Web 12/14/2006

remain poorly understood as well as how these details vary with changing environmental conditions. The quantum yields of MSA, SO_2, and other particle precursors are mechanism dependent, and thus accurate interpretation of paleoclimatic data and assessments of anthropogenic perturbations to the atmospheric sulfur cycle rely on kinetic and mechanistic details of natural sulfur chemistry.

In remote regions of the MBL where NO_x concentrations are typically low, DMS oxidation proceeds largely by eq 1. Kinetic studies have often focused on this equation and its deuterated analog, eq 2.

$$CH_3SCH_3 + OH \rightarrow \text{products} \quad (1)$$

$$CD_3SCD_3 + OH \rightarrow \text{products} \quad (2)$$

The observed or "effective" rate coefficient for the reaction of OH with h_6-DMS and d_6-DMS has been shown to depend on the partial pressure of O_2.[13,14,16,18−20] In the absence of O_2, the reaction shows no pressure dependence, positive activation energy, and a kinetic isotope effect. These observations are consistent with H-atom abstraction from the methyl groups. However, an enhancement in the rate coefficient is observed in the presence of O_2. This rate enhancement has a negative activation energy, pressure dependence, and shows no kinetic isotope effect, behavior consistent with an addition process. Hynes et al.[18] proposed a two-channel mechanism of oxidation, involving direct hydrogen abstraction, together with reversible formation of the OH−DMS adduct which is scavenged by molecular oxygen, written below for both h_6-DMS and d_6-DMS.

h_6-DMS

$$CH_3SCH_3 + OH \rightarrow CH_2SCH_3 + H_2O \quad (1a)$$

$$CH_3SCH_3 + OH \leftrightarrow CH_3S(OH)CH_3 \quad (1b/-1b)$$

$$CH_3S(OH)CH_3 + O_2 \rightarrow \text{products} \quad (3)$$

d_6-DMS

$$CD_3SCD_3 + OH \rightarrow CD_2SCD_3 + HOD \quad (2a)$$

$$CD_3SCD_3 + OH \leftrightarrow CD_3S(OH)CD_3 \quad (2b/-2b)$$

$$CD_3S(OH)CD_3 + O_2 \rightarrow \text{products} \quad (4)$$

In this mechanism, the branching between abstraction (1a or 2a) and addition (1b or 2b) is temperature dependent, and the forward addition reaction is pressure dependent, giving a complex temperature dependence for both the effective rate and the branching ratio between the addition and abstraction channels. Elementary rates were inferred in Hynes et al.,[18] and the results were well described by a value for $k_{1b} = 1.3 \times 10^{-11}$ cm^3/molec-s at 760 torr. Adduct equilibration (1b/−1b or 2b/−2b) was not directly observed in that work, yet the two-channel mechanism has been widely accepted as the operative mechanism for the OH-initiated oxidation of DMS in the marine boundary layer and, until recently, the directly determined rates and inferred branching ratios of Hynes et al.[18] were recommended as the best available for tropospheric modeling.[21−24]

Subsequent, direct observations of the equilibration[11,14] were in reasonable agreement for the values of k_{2b}, K_c, and adduct binding energy at low pressures. However, studies from this laboratory[12,25−27] are not consistent with $k_{1b} = 1.3 \times 10^{-11}$ cm^3/molec-s at 760 Torr. Williams et al.[26] showed that the 1986 expression for the effective rate coefficient for eq 1, k_{obs}, underestimates the overall rate of oxidation as well as the branching ratio by a factor of 2 at low temperature. The latest IUPAC recommendation[22] for k_{obs} is a parametrization of that data[13] and Albu et al.[16] recently presented results from a relative rate study in good agreement with the work of Williams et al.

The DMS(OH) adduct can react with O_2 to form various potential product combinations.[18]

$$CH_3S(OH)CH_3 + O_2 \rightarrow CH_3S(O)CH_3 + HO_2 \quad (3a)$$

$$CH_3S(OH)CH_3 + O_2 \rightarrow CH_3S(O_2)CH_3 + OH \quad (3b)$$

$$CH_3S(OH)CH_3 + O_2 \rightarrow CH_3SOH + CH_3O_2 \quad (3c)$$

Adduct reaction with oxygen produces HO_2 (3a) with a yield of 50%.[15,28] $DMSO_2$ has also been detected in chamber studies,[19,29−32] suggesting that eq 3b could also contribute significantly to final product yield. However, $DMSO_2$ may also be produced by the rapid oxidation of DMSO by OH in the presence of O_2. So, eq 3b is not required to explain the observations in chamber studies. If this reaction is a significant channel of 3 or 4, then OH is regenerated and any kinetic measurement technique that relies on temporal monitoring of OH radicals would not observe eq 3b and would measure a rate coefficient that is too slow. Hence, discrepancies between relative rate studies[19,20] and direct studies[14,18,25] could be resolved if OH regeneration is significant. Continued inability to model field observables on the basis of the current understanding of kinetics demonstrates that the parametrization of this process for atmospheric conditions is incomplete.[33−35]

There have also been a large number of computational studies[34−38] of both channels of eq 1, producing contradictory results particularly for the adduct formation channel. We have performed a series of experimental and computational studies of the reactions of OH with DMS, its fully deuterated isotopomer, d_6-DMS, and several higher alkanes. The electronic structure calculations use Gaussian 03 and focus on DMS(OH) adduct formation. We report direct observations of the rate coefficients for the formation and dissociation of the h_6-OHDMS and d_6-OHDMS adducts over the pressure range 50−650 Torr and between 240 and 245 K, together with measurements of the oxygen dependence of the effective rate coefficients for eqs 1 and 2 under similar conditions. This has allowed us to characterize the pressure and temperature dependence for all of the elementary processes in the initial steps of the DMS oxidation mechanism at low temperature and to estimate the effects of OH regeneration on the kinetics. We also present the results of our calculations on the structure and stability of the h_6-OHDMS and d_6-OHDMS adducts. Our results for the higher alkyl sulfides will be reported in subsequent publications.

Experimental

A pulsed laser photolysis−pulsed laser-induced fluorescence (PLP-PLIF) system was used to generate OH radicals in situ, monitor their decay in real time, and thereby measure the elementary rates for sulfide oxidation. The system is similar to one described for other kinetic studies performed in this laboratory.[12,13,39−41]

Experiments were performed in a thermostated Pyrex reaction cell equipped with a chromega-alomega (K-type) thermocouple inserted through a vacuum seal into the reaction zone. Photolysis and probe beams were combined by a dichroic mirror and were propagated into the cell perpendicular to both the direction of gas flow and the detection source. OH was produced by the pulsed laser photolysis of H_2O_2 at 266 nm using the fourth

harmonic output from an Nd:YAG laser (Quanta-Ray GCR-16). Initial radical concentrations were typically $\sim 1 \times 10^{12}$ cm^{-3}. Pulsed laser-induced fluorescence using an Nd:YAG pumped, frequency doubled, tunable dye laser (Quanta-Ray DCR-3, Quanta-Ray PDL-3) was used for OH detection. Excitation was via the Q_1 1 line of the $A^2\Sigma - X^2\Pi$ (1−0) transition at 282 nm. Fluorescence was detected with a photomultiplier tube outside a third arm, after passing through a lens and collection optics optimized to discriminate against Rayleigh and Raman scattering from N_2 and O_2. Fluorescence in the 0−0 and 1−0 bands was detected at 308 nm. Photomultiplier output was amplified, appropriately terminated, and processed by a 500 MHz digital oscilloscope to obtain the area of the fluorescence signal, averaged for typically 50 laser shots.

Kinetic information was obtained by varying the delay time between photolysis and probe beams with a digital delay generator. Signal was collected for usually 20 delays over an OH temporal profile, spanning 2−3 orders of magnitude. Experiments were carried out under "slow-flow" conditions, with flows in the range 5−10 cm/s. All flows were monitored using calibrated mass flow-meters, and pressure was monitored throughout the system using Baratron capacitance monometers.

Sulfide concentrations were measured in situ both before and after the reaction cell using UV photometry. Values for the cross sections were determined in this laboratory.[42] Sulfide losses in the reaction cell at all temperatures were less than 5% and O_2 concentrations were calculated from flows.

Results

Data Analysis. Experiments and analysis for both isotopomers are based on the assumption that oxidation proceeds via the two-channel mechanism. A kinetic analysis of the system described above is greatly simplified if both pseudo-first-order conditions and the steady-state approximation as applied to the adduct are valid, that is, [DMS] ≫ [OH] ≫ [DMS(OH)]. Under these conditions, OH temporal profiles will always show single exponential behavior, and a plot of the pseudo-first-order decay rate, k', versus DMS concentration will be linear with a slope k_{obs}. An expression for the overall observed rate for oxidation, k_{obs}, as a function of the elementary rates and the concentration of $[O_2]$ at any fixed pressure [M] is given in eq I.

$$k_{obs} = \frac{k_a + \frac{k_s}{k_b}(k_a + k_f)[O_2]}{1 + \frac{k_s}{k_b}[O_2]} \qquad \text{(I)}$$

where k_a is the abstraction rate coefficient, $k_a = k_{1a}$ or k_{2a}. k_f is the effective second-order rate coefficient for adduct formation, $k_f = k_{1b}$ [M] or k_{2b} [M]. k_b is the unimolecular rate coefficient for adduct decomposition, $k_b = k_{-1b}$ or k_{-2b}, and k_s is the rate coefficient for adduct "scavenging", that is, reaction with O_2, $k_s = k_3$ or k_4. Consequently, the effective oxidation rate, k_{obs}, will vary both as a function of total pressure and as a function of oxygen partial pressure at any fixed total pressure [M]. Equation I indicates that k_{obs} has two limiting values. In the absence of O_2, observed OH loss is due only to the abstraction channel and $k_{obs} = k_a$. Equation I predicts that an increase in O_2 partial pressure, at a fixed total pressure, results in an increase in k_{obs} as OH−DMS is scavenged rather than decomposing back to reactants. The effective rate coefficient increases, as the contribution of k_f increases, until it asymptotically approaches a limiting rate, which is the sum of the rate coefficients for abstraction and adduct formation. Hence, at this limiting value of k_{obs}, $k_{obs} = k_a + k_f$. When the limiting rate is reached, each adduct produced is scavenged by O_2, and a further increase in the partial pressure of O_2 results in no increase in k_{obs}. The magnitude of k_f defines the maximum enhancement possible for k_{obs} in the presence of $[O_2]$, and observation of this limiting value of k_{obs} gives a direct measurement of k_f. At low temperatures, the limiting rate can be observed at lower oxygen concentration since increased adduct lifetime allows more time for reactive collisions with O_2 to occur. This behavior is indeed observed[11,13,14,18−20] and has been exploited in experiments presented in section 2.

At high concentrations of [DMS], the equilibrium of k_f/k_b shifts to the right, the steady-state approximation breaks down, and biexponential OH decays can be observed if experimental time resolution is adequate.[14,25,41] As long as pseudo-first-order conditions are maintained, that is, [DMS] ≫ [OH], OH temporal profiles are described by eq II.

$$\frac{[OH]_t}{[OH]_0} = \frac{(K + \lambda_1)\exp(\lambda_1 t) - (K + \lambda_2)\exp(\lambda_2 t)}{\lambda_1 - \lambda_2} \qquad \text{(II)}$$

$$K = k_b + k_s[O_2] \qquad \text{(III)}$$

$$\lambda_1 = 0.5[(\alpha^{2^-} 4\beta)^{1/2} - \alpha] \qquad \text{(IV)}$$

$$\lambda_2 = -0.5[(\alpha^{2^-} 4\beta)^{1/2} + \alpha] \qquad \text{(V)}$$

$$\alpha = K + (k_a + k_f)[DMS] \qquad \text{(VI)}$$

$$\beta = (k_a K + k_b k_s[O_2])[DMS] \qquad \text{(VII)}$$

The observed OH temporal profiles can be fit with eq II to obtain elementary rate coefficients.

1. Formation of h_6-DMS−OH and d_6-DMS−OH Adducts. Experiments were performed in N_2 buffer gas at 100−600 Torr total pressure with sulfide concentrations ranging from 1×10^{15} to 7.5×10^{16} molecules cm^{-3}. The cell temperature was approximately 240 K, the lowest temperature we could achieve using H_2O_2 as an OH precursor. In practice, the gas temperature in the reaction zone varied between 239 K and 245 K and data were obtained over this range. Typical OH decays in 500 Torr of N_2 and at 240 K are shown for h_6-DMS in Figure 1 and in 100 Torr N_2 and at 240 K for d_6-DMS in Figure 2. OH temporal profiles initially show a very rapid decrease because of equilibration and a slower loss of OH over longer time scales because of hydrogen/deuterium abstraction. Equilibration takes place on a time scale of ~4 μs for both sulfides at pressures of 100 Torr and on a time scale of ~1 μs at 500 Torr. Figure 3 shows a plot of the residuals for both data sets. Residuals are larger at an extremely short time as expected but there is no bias. The scatter associated with the higher pressure data is larger, and this reflects the lower signal-to-noise ratio at higher pressures which is primarily due to more efficient fluorescence quenching.

Double exponential decays were analyzed by a Levenson-Marquardt type, unweighted, least mean squares fit of the data to eq II which took relative values of the OH concentration as a function of delay time and fit to values of $[OH]_0$, K, λ_1, and λ_2. Rates of diffusion out of the reaction zone of either OH or the adduct were considered to be negligible compared to the time scales of equilibration and abstraction and were ignored.[11] Single decays were analyzed to yield elementary rate coefficients for k_a, k_f, and k_b for several sulfide concentrations at each

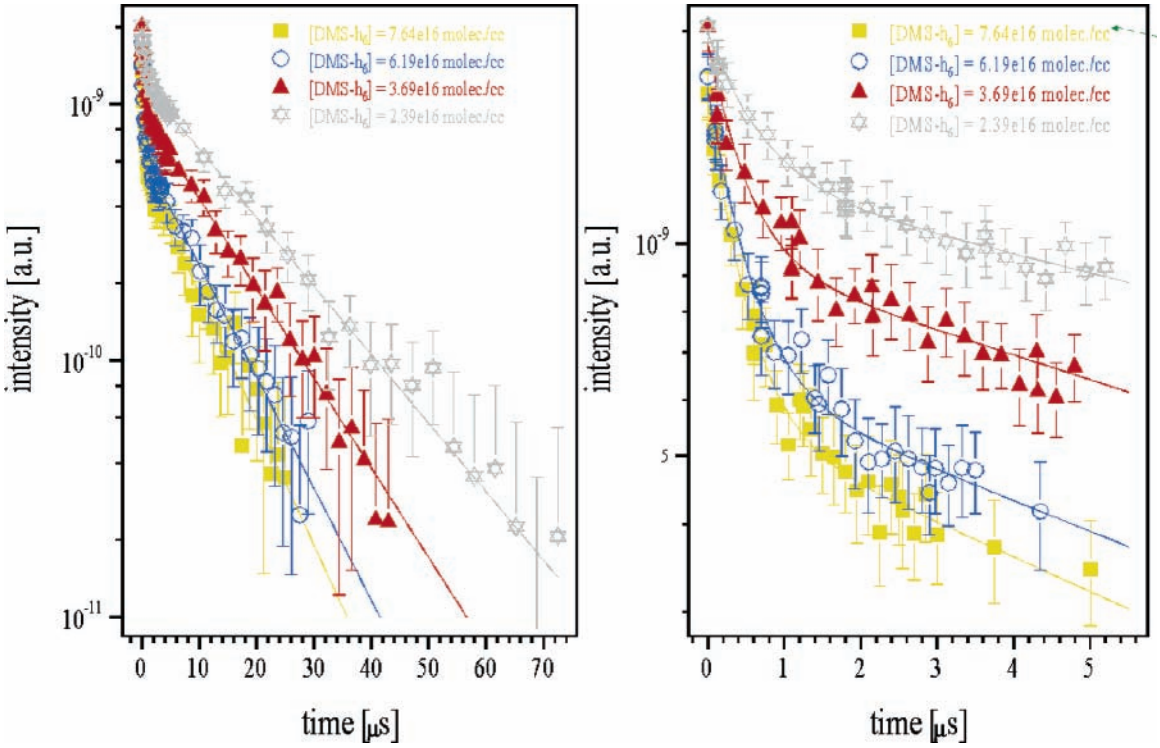

Figure 1. Typical OH decays in the presence of excess h_6-DMS at 500 Torr total pressure of N_2 and 245 K.

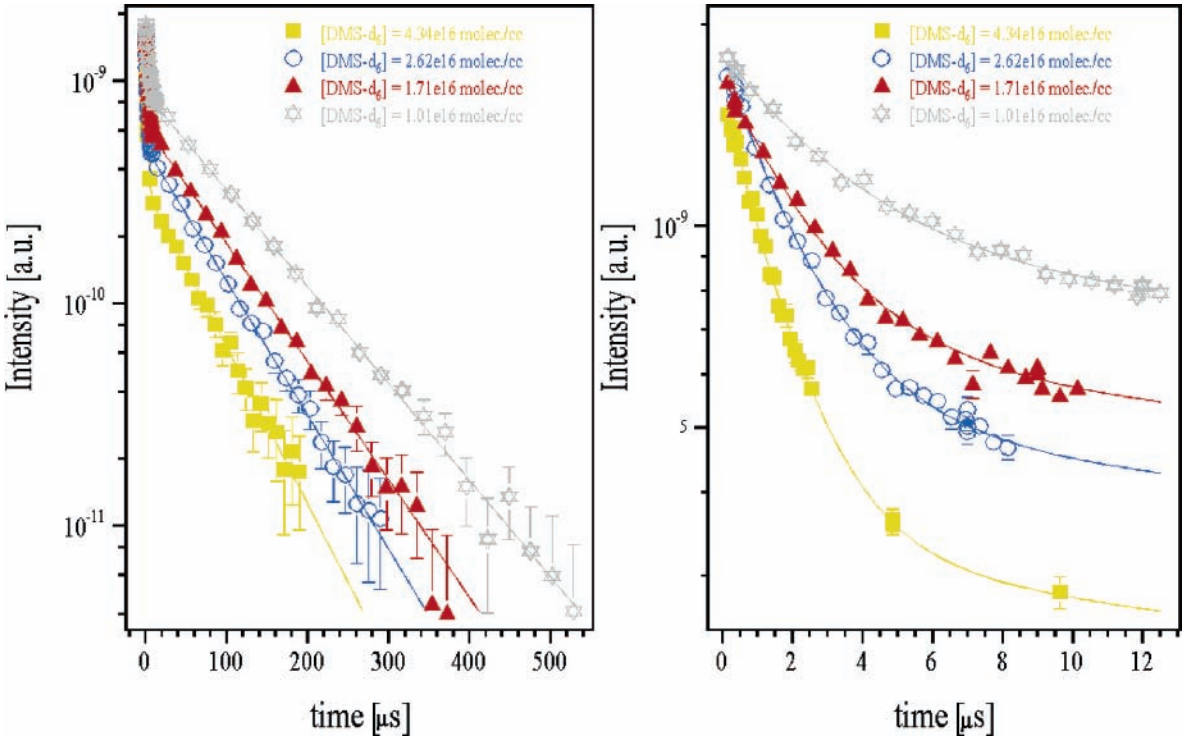

Figure 2. Typical OH decays in the presence of excess d_6-DMS at 100 Torr total pressure of N_2 and 240 K.

pressure. The values of these rate coefficients were then averaged to give the values for that pressure. In addition, the elementary rate coefficients were obtained by plotting alpha and beta against [DMS] at each pressure. Figure 4 shows a typical plot of alpha versus [DMS]. The analyses were in good agreement with each other, and plots of alpha and beta against [DMS] were used to obtain the elementary rates reported in Table 1. Values of k_f obtained from the averages of single-decay analysis did not differ more than 5% from the "bulk" analysis. As an additional test, independently determined abstraction rates were used in these calculations in lieu of k_{1a} and k_{2a} determined from the biexponential OH decay. Again, rates of forward addition did not change by more than 5%. Despite being least sensitive to the abstraction rate with this method, average values of k_a for both sulfides were in good agreement with prior literature values.

Figures 5 and 6 show plots of the rate coefficient for adduct formation, k_f, as a function of pressure for h_6-OHDMS and d_6-OHDMS, and these will be discussed in detail below. Having obtained values for the forward and reverse rate coefficients

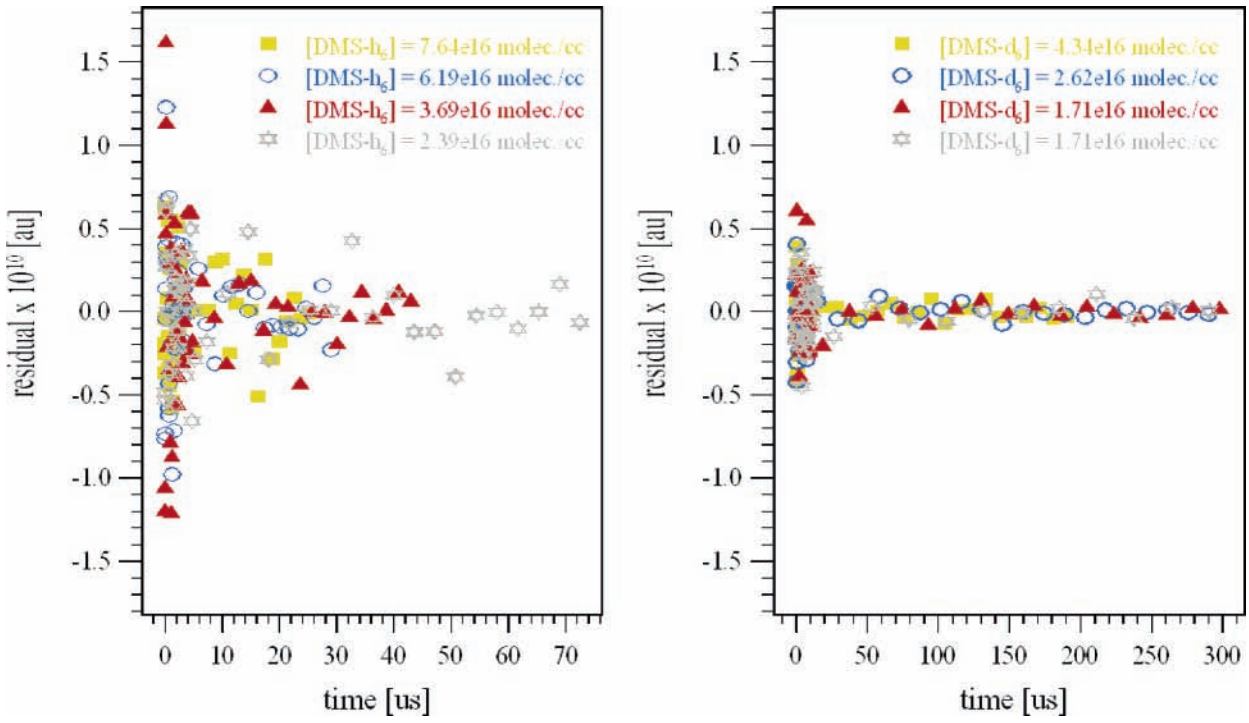

Figure 3. Residuals to the fits shown in Figures 1 and 2.

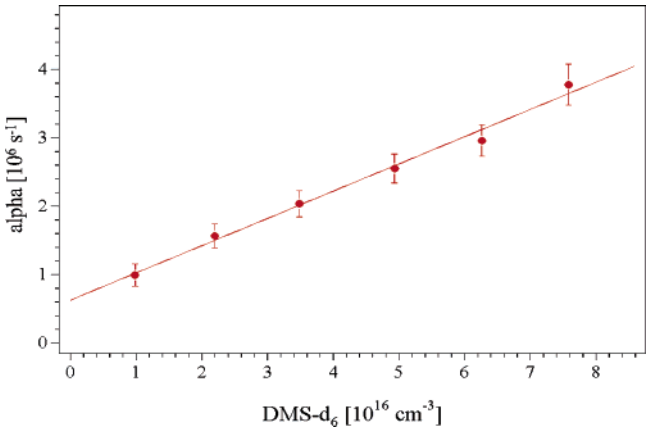

Figure 4. Typical plot of α as a function of [DMS]. According to eq VI, the slope gives the sum of abstraction and addition reactions.

for adduct formation, we can calculate values of the equilibrium constant, K_c. As noted above, data were obtained over a small temperature range. We estimate the uncertainty in the temperature in the reaction zone to be approximately 0.5 K on the basis of temperature profiles of the reaction cell, and hence the measurements were grouped around temperatures of 240.0 ± 1 K, 242.5 ± 1 K, and 245.0 ± 1.0 K, and the average of each group was taken and reported in Table 1 along with the errors of the average. A considerable amount of scatter is observed in elementary rate data obtained from fits to eq II. This reflects partially the data quality due to the difficult nature of the experiments as well as the inherent problem of extracting three rate parameters, two of which are of similar magnitude, from a single, nonlinear decay.[11] The fitting routine uses four parameters and is best defined when $[OH]_0$, both slopes, and the point between the two slopes are well defined. Conditions that optimize the above parameters, that is, increased pressure and decreased temperature, also maximize signal quenching and H_2O_2 loss, potentially limiting data precision and dynamic range. This is the first report of equilibration measurements in N_2 above 100 Torr. The measurements, when viewed in conjunction with O_2 measurements discussed in the following sections, are completely consistent with the simple two-channel mechanism detailed above.

Equilibrium constants for both sulfides are shown as a function of pressure in Figure 7 at three temperatures. Values of the equilibrium constants for both sulfides are identical within the 2σ errors of precision and as expected show no pressure dependence. Values of the equilibrium constant can be compared with our previous results which were obtained at higher temperatures and a single pressure, 100 Torr of N_2, for d_6-DMS only.[11] The van't Hoff equation relates the temperature dependence of the equilibrium constant to reaction enthalpy, assuming that ΔH and ΔS are independent of temperature.

$$\ln K_p = (\Delta S/R) - (\Delta H/RT) \qquad \text{(VIII)}$$

Hence, the slope of the plot of ln K_p versus T^{-1}, where $K_p(RT) = K_c$, gives the exothermicity of reaction, the adduct binding energy. The *y*-intercept gives the entropy change for the reaction. Figure 8 shows a van't Hoff plot of the current work and our previous data for d_6-DMS,[11] and the solid line shows the best fit to the combined data set and gives $\Delta H^o = -10.9 \pm 1.0$ kcal mol^{-1} and $\Delta S^o = -31 \pm 4$ cal mol^{-1} K^{-1} over the temperature range 267−240 K. The adduct bond strength of 10.9 kcal mol^{-1} is in good agreement with the previous value of 13.0 ± 3.3 kcal mol^{-1}. For comparison, the 100 Torr N_2 data of Barone et al.[14] are also shown. A "third law calculation" of the enthalpy change at 240 K utilizes the entropy change calculated from the computed vibrational frequencies, $\Delta S_{240K}^o = -29.5$ cal mol^{-1} K^{-1}. Taking a value of $K_{p,240K} = 1415$ from the van't Hoff expression gives an enthalpy change, $\Delta H_{240K}^o = -10.5$ kcal mol^{-1}. The value of ΔH was corrected to give the value at 298 K using heat capacities calculated from the vibrational frequencies. Using a calculated $\Delta C_{p,240} = 1.8$ cal mol^{-1} K^{-1}, we obtain $\Delta H_{rxn,\ 298K}^o = -10.4$ kcal mol^{-1}. A discussion of the errors associated with these calculations was presented in Hynes et al.,[18] and we estimate the uncertainty in $\Delta H_{rxn,\ 298K}^o$ as ±1 kcal mol^{-1}. Comparison with the binding energies

TABLE 1: Elementary Rates and Equilibrium Constants Measured in This Work and Associated Experimental Conditions

sulfide	*P* (Torr)	*T* (K)	k_f (10^{-11}) cm^3/molec.-s	k_b (10^5) cm^3/molec.-s	k_a (10^{-12}) cm^3/molec.-s	K_C (10^{-17})	*T* (K) average	K_C (10^{-17}) average
DMS-h_6	200	244.7	(0.89 ± 0.13)	(3.77 ± 0.15)	(3.55 ± 0.69)	(2.36 ± 0.45)	245.4	(2.18 ± 0.22)
	300	244.7	(1.16 ± 0.17)	(4.86 ± 0.69)	(3.76 ± 1.08)	(2.38 ± 0.69)		
	400	245.7	(1.48 ± 0.06)	(7.25 ± 0.22)	(3.47 ± 0.20)	(2.04 ± 0.14)		
	500	246.6	(1.98 ± 0.39)	(9.97 ± 1.65)	(3.24 ± 1.26)	(1.99 ± 0.72)		
	600	245.0	(1.97 ± 0.34)	(8.22 ± 1.32)	(4.29 ± 1.29)	(2.40 ± 0.80)		
	650	245.4	(1.89 ± 0.53)	(9.76 ± 2.92)	(3.44 ± 3.18)	(1.94 ± 1.12)		
	50	239.0	(0.25 ± 0.03)	(0.68 ± 0.13)	(6.65 ± 3.11)	(3.71 ± 5.51)	240.3	(5.67 ± 2.02)
	100	240.6	(0.9 ± 0.16)	(1.11 ± 0.10)	(5.55 ± 1.01)	(8.19 ± 2.21)		
	200	240.7	(1.12 ± 0.26)	(2.52 ± 0.39)	(4.50 ± 1.80)	(4.44 ± 1.71)		
	100	240.8	(0.76 ± 0.06)	(1.22 ± 0.07)	(3.8 ± 0.40)	(6.36 ± 0.87)		
	500	242.0	(2.30 ± 0.19)	(5.32 ± 0.35)	(4.07 ± 0.53)	(4.32 ± 0.64)	242.4	(4.10 ± 0.50)
	400	242.0	(1.63 ± 0.49)	(4.71 ± 1.01)	(9.05 ± 3.60)	(3.46 ± 1.77)		
	300	242.1	(1.76 ± 0.22)	(3.95 ± 0.39)	(4.54 ± 0.91)	(4.46 ± 1.01)		
	300	242.5	(1.40 ± 0.12)	(3.90 ± 0.27)	(3.92 ± 0.50)	(3.59 ± 0.56)		
	600	242.8	(2.27 ± 0.22)	(5.63 ± 0.87)	(5.90 ± 1.51)	(4.03 ± 1.00)		
	600	242.9	(2.62 ± 0.15)	(5.53 ± 0.36)	(3.95 ± 0.65)	(4.74 ± 0.57)		
DMS-d_6	100	244.5	(0.75 ± 0.17)	(2.74 ± 0.67)	(1.15 ± 0.75)	(2.76 ± 1.29)	244.9	(2.14 ± 0.42)
	200	244.5	(1.15 ± 0.12)	(5.03 ± 0.81)	(1.40 ± 0.47)	(2.29 ± 0.61)		
	300	245.2	(1.60 ± 0.10)	(7.75 ± 0.61)	(1.28 ± 0.27)	(2.06 ± 0.30)		
	400	245.5	(1.70 ± 0.29)	(10.3 ± 1.60)	(0.66 ± 0.45)	(1.65 ± 0.54)		
	500	244.7	(2.19 ± 0.92)	(11.2 ± 3.10)	(4.79 ± 11.6)	(1.95 ± 1.35)		
	600	241.0	(3.76 ± 0.10)	(6.26 ± 0.37)	(1.89 ± 0.17)	(6.01 ± 0.52)	241.5	(5.05 ± 1.36)
	300	242.1	(1.94 ± 0.16)	(4.75 ± 0.71)	(1.74 ± 0.47)	(4.08 ± 0.96)		
	100	240.5	(1.08 ± 0.07)	(1.47 ± 0.08)	(1.46 ± 0.14)	(7.36 ± 0.94)	240.1	(6.18 ± 1.68)
	400	239.8	(2.81 ± 0.20)	(5.63 ± 0.40)	(1.42 ± 0.20)	(4.99 ± 0.72)		

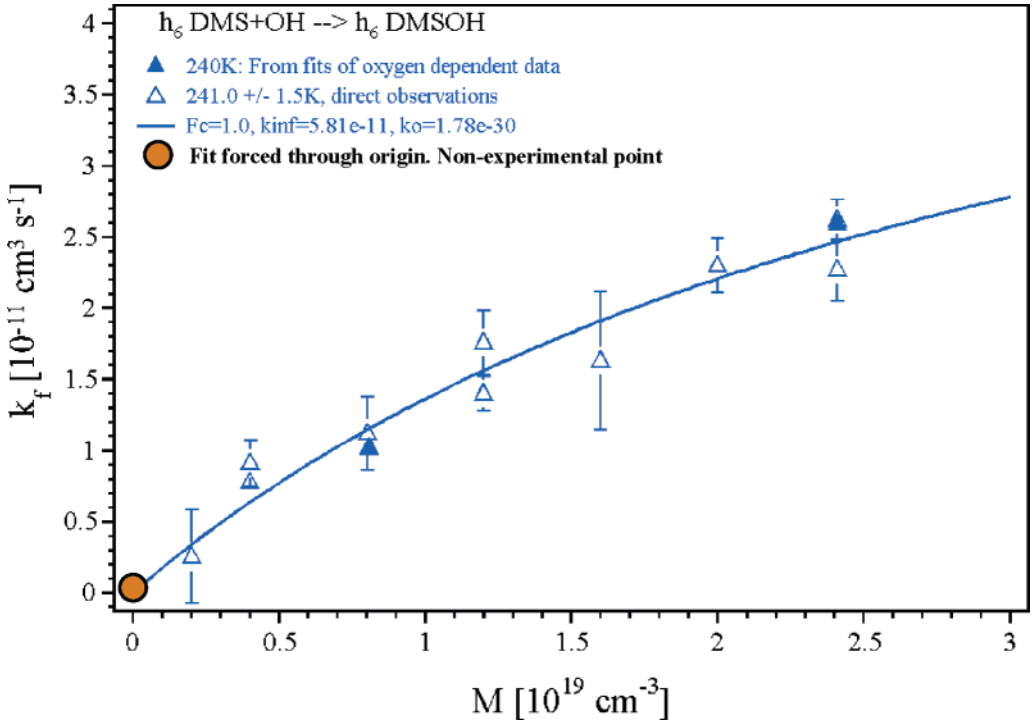

Figure 5. Rates of h_6-OHDMS adduct formation k_f ($k_f = k_{1b}$) as a function of pressure. Open triangles are determined from fits of eq II to biexponential OH decays. Solid triangles are determined from fits of eq I to oxygen-dependent data discussed in section 2. All points are fit with a Troe parametrization, eq X (solid line). When F_c is fixed at a value 1.0, $k_\infty = 5.82e - 11$ cm^3/molec-s and $k_0 = 1.78e - 30$ cm^6/molec^2-s.

obtained from the electronic structure calculations shows that they underestimate the stability of the OH−DMS adduct.

2. Observations in the Presence of O_2. Experiments in the presence of O_2 are limited to conditions where [OH] ≫ [OH−DMS] and the steady-state approximation is valid. Under these conditions, OH temporal profiles show single exponential behavior, and plots of pseudo-first-order decay rates (k') against [h_6-DMS] or [d_6-DMS] give the effective rate coefficient, k_{obs}, defined by eq I. Experiments were performed at ∼240 K, as a function of O_2 partial pressure and at fixed total pressures of 200 and 600 Torr with N_2 as the buffer gas. The 600 Torr data were reported in a preliminary account of this work.[13] All second-order rate constants are listed in Tables 2a and 2b with experimental conditions. Figure 9 shows typical OH temporal profiles at 200 Torr total pressure demonstrating the expected single exponential behavior. Figure 10 shows the variation in pseudo-first-order decay rate with [h_6-DMS], at 200 Torr total pressure and several O_2 partial pressures. We see the expected linear dependence of k' on [DMS], the slope of which is used to obtain k_{obs}, together with a strong dependence of k_{obs} on the O_2 partial pressure. Figures 11 and 12 show the variation in the effective rate coefficient, k_{obs}, of eqs 1 and 2 with oxygen

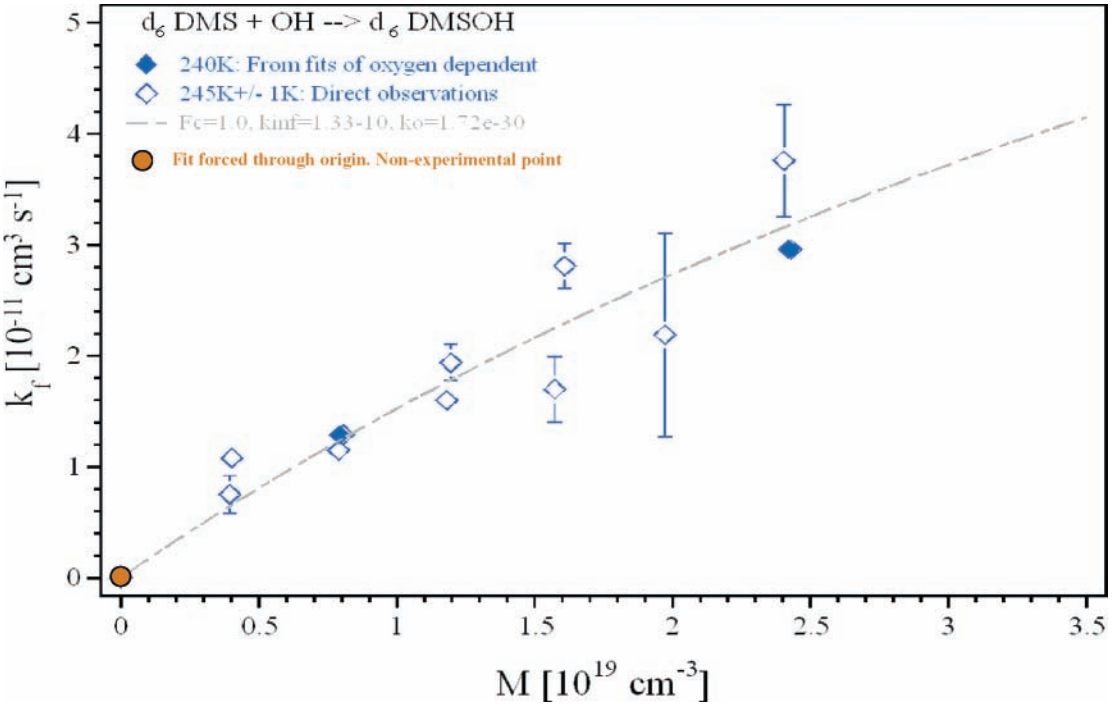

Figure 6. Rates of d_6-OHDMS adduct formation k_f ($k_f = k_{2b}$) as a function of pressure. Open diamonds are determined from fits of eq II to biexponential OH decays. Solid diamonds are determined from fits of eq I to oxygen-dependent data discussed in section 2. All points are fit with a Troe parametrization, eq X, (dashed line). When F_c is fixed at a value of 1.0, $k_\infty = 1.33e - 10$ cm^3/molec-s and $k_0 = 1.72e - 30$ cm^6/molec^2-s.

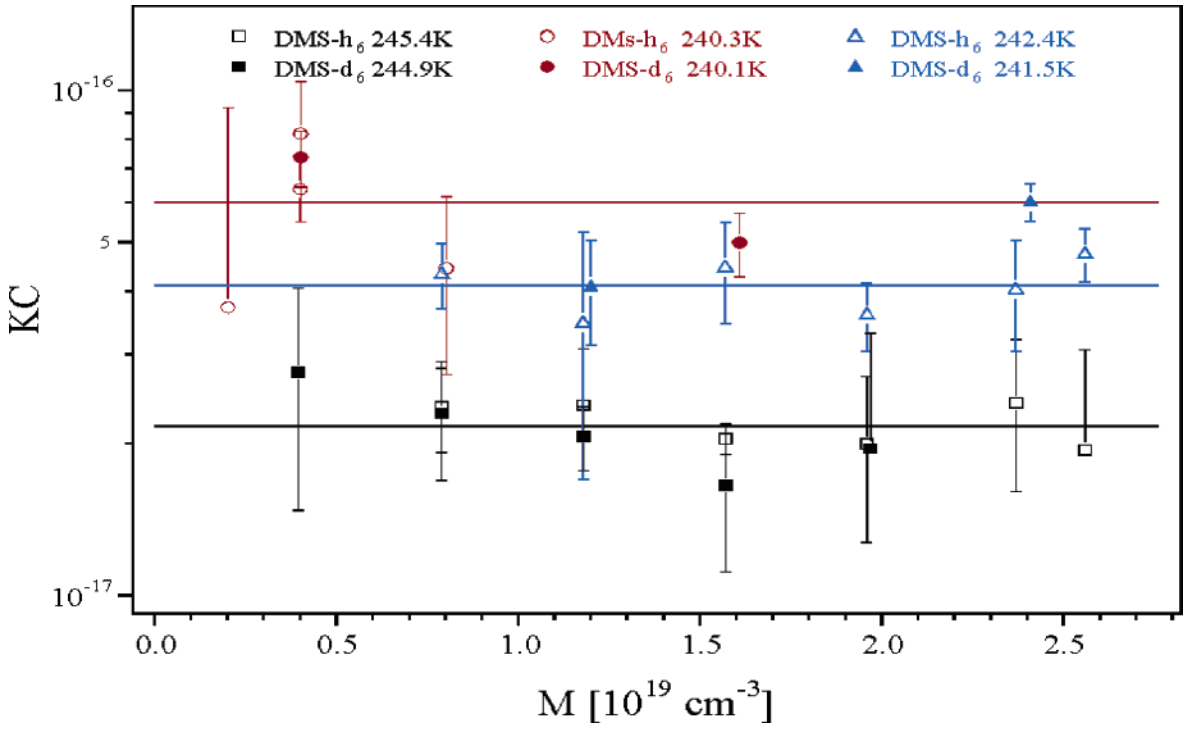

Figure 7. Equilibrium (k_f/k_b) constants as a function of pressure for the formation of both adducts (h_6-OHDMS and d_6-OHDMS) at various temperatures. No pressure dependence is apparent within the error of the measurements or difference between the two isotopomers at a given T. Despite significant error bars and small temperature range, it is apparent that K_C 245 K < K_C 242 K < K_C 240 K.

partial pressure at total pressures of 200 and 600 Torr. At 0% O_2, no difference is seen between the 200 and 600 Torr data because the abstraction rate is pressure independent. For both reactions, it can be seen that, as the O_2 partial pressure increases, k_{obs} increases and that the "O_2 enhancement" is larger at higher total pressures. This is due to the pressure dependence of the rate coefficient for adduct formation, k_f.

The oxygen-dependent data were analyzed using eq I. The values of the equilibrium constant, determined in the equilibration measurements presented in section 1, and the abstraction rate coefficient, measured in the absence of O_2, were fixed parameters. The rate coefficients for adduct formation and adduct reaction with O_2 were adjusted to provide the best fits to the "roll off" data. In this approach, k_b does not appear

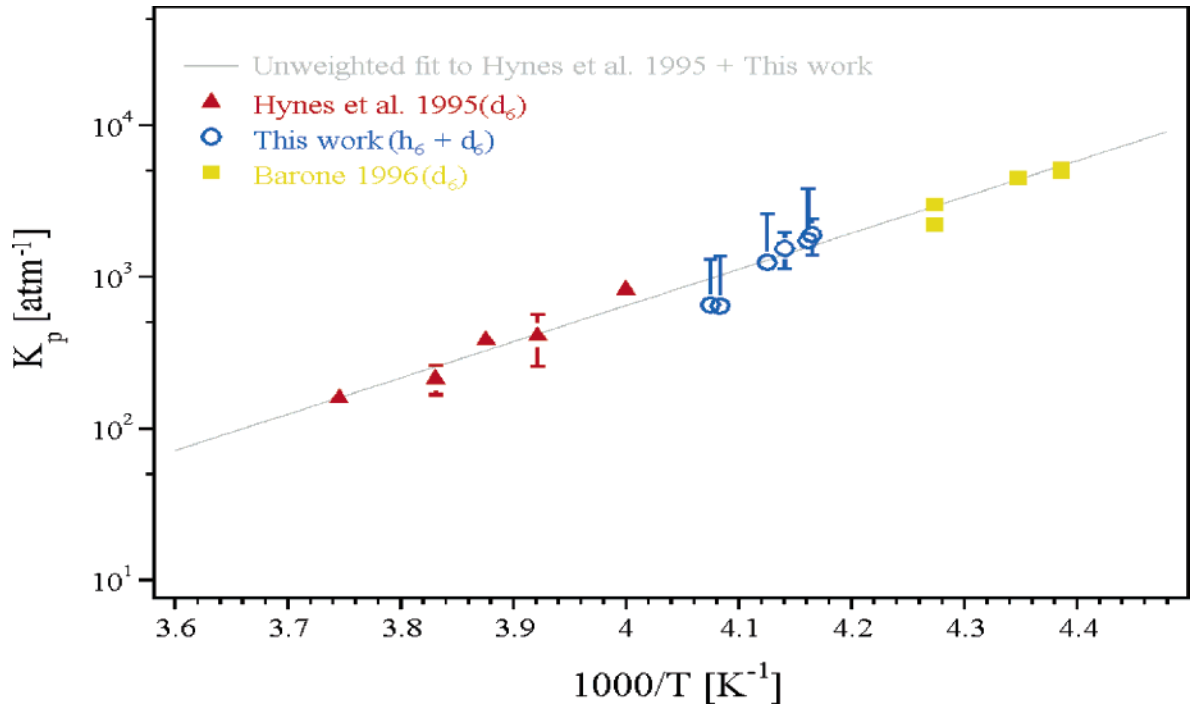

Figure 8. van't Hoff relationship (eq VIII) for k_{1b}/k_{-1b} and k_{2b}/k_{-2b} determined in this work shown together with data from Hynes et al.[11] and Barone et al.[14] The solid line is an unweighted, least-squares linear fit of eq VIII to the data of Hynes et al.[11] and this work. Error bars are the 2σ errors of precision of the individual measurements.

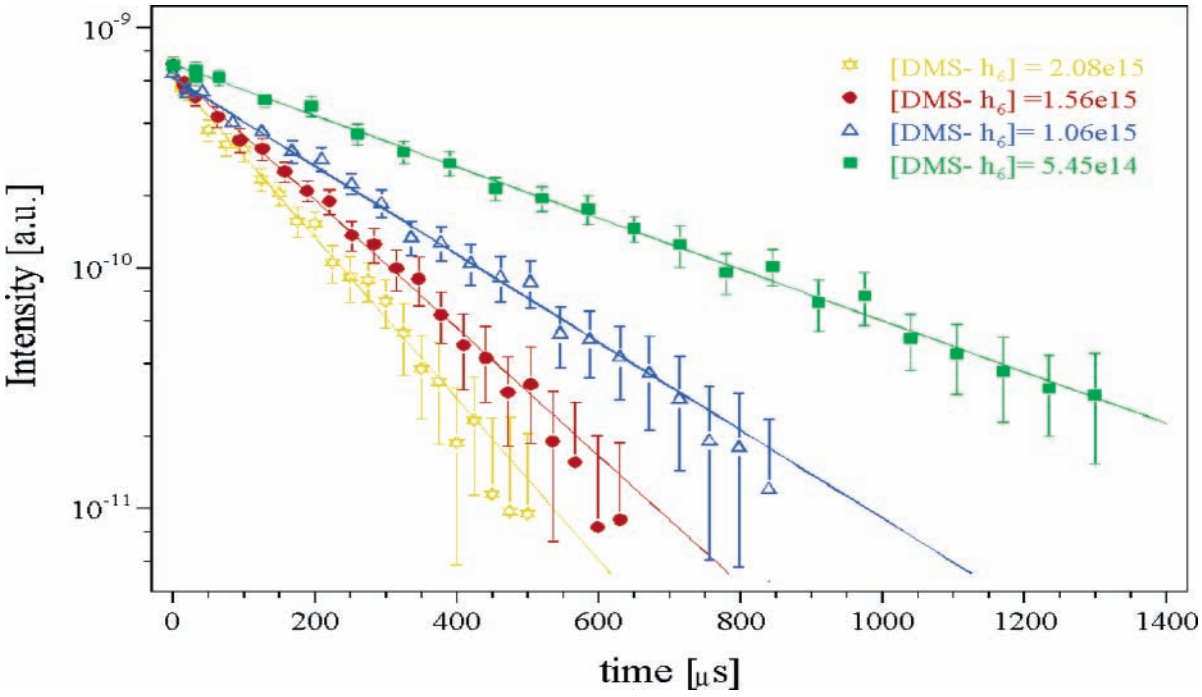

Figure 9. Typical OH temporal profiles at 200 Torr total pressure ($N_2 + O_2$) and 240 K. [h_6-DMS] remained low enough that OH decays showed single exponential behavior.

explicitly in eq I but is replaced by K_c/k_f.

$$k_{obs} = \frac{k_a + \frac{K_c * k_s}{k_f}(k_a + k_f)[O_2]}{1 + \frac{K_c * k_s}{k_f}[O_2]} \qquad \text{(IX)}$$

The dashed lines in Figures 11 and 12 show the best fits to the data using the values of K_c taken from the van't Hoff dependence (Figure 8). The values of k_f and k_s obtained from the best fits are shown in Table 3 when k_s and k_f are both free parameters. Figures 11 and 12 also show the ability of the expression discussed in section 3 of the Discussion to predict the oxygen dependence of eqs 1 and 2. Figures 11 and 12 show that eq I can quantitatively explain the dependence of k_{obs} on $[O_2]$. As we discuss below, the values of k_f derived from these measurements agree well with values determined independently from equilibration measurements. Although the rate of adduct

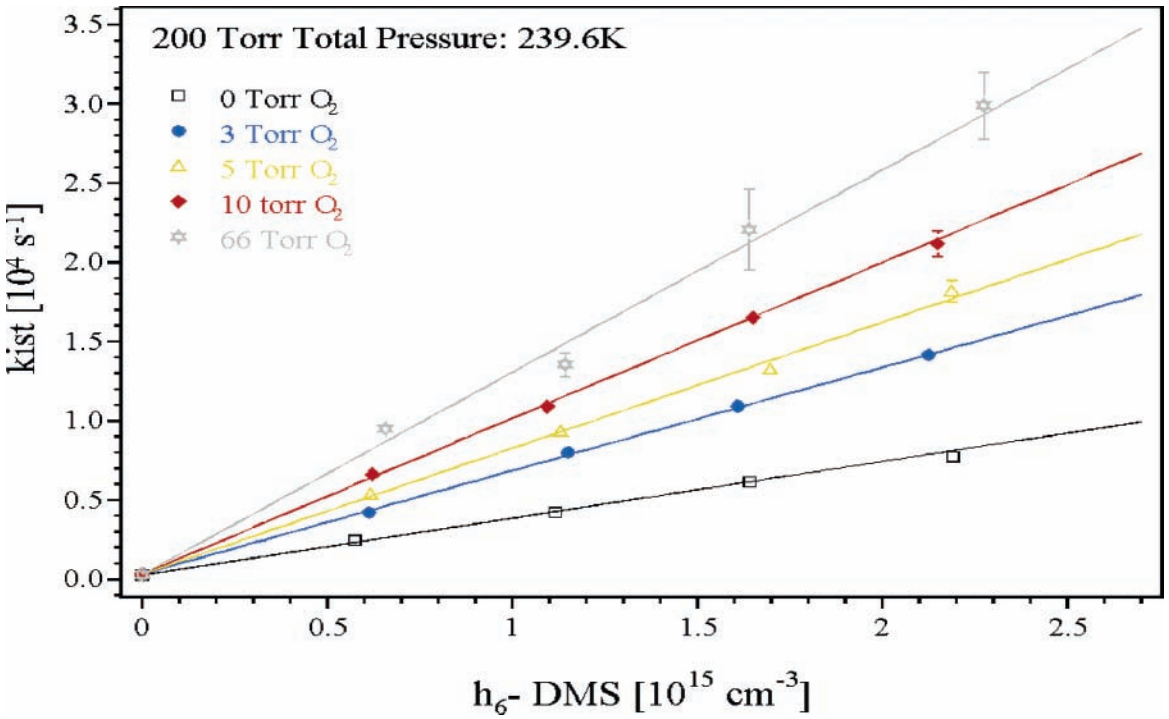

Figure 10. Variation in pseudo-first-order decay rate (k') with [h_6-DMS] at 200 Torr total pressure ($N_2 + O_2$) and various partial pressures of O_2. The slope of the linear relationship between k' and [DMS] gives k_{obs} which is strongly dependent on the partial pressure of O_2.

TABLE 2: Summary of Overall Bimolecular Rate Constants as a Function of Pressure and Partial Pressure of Oxygenn

sulfide	total P (Torr) $N_2 + O_2$	partial P (Torr) O_2	T (K)	range of k' (s^{-1})	k_{obs} (cm^3/molec-s)
		Equation 1			
h_6-DMS	200	0	239.7	258−7738	(3.59 ± 0.07)e − 12
	200	3	239.5	330−14 148	(6.52 ± 0.10)e − 12
	200	5	239.3	321−18 150	(7.94 ± 0.15)e − 12
	200	10	239.5	311−21 192	(9.83 ± 0.18)e − 12
	200	20	240.1	289−24 878	(1.11 ± 0.03)e − 11
	200	40	239.8	276−26 102	(1.22 ± 0.03)e − 11
	200	66	239.5	348−26 811	(1.27 ± 0.04)e − 11
	200	100	239.7	289−29 900	(1.28 ± 0.04)e − 11
	600	0	241.5	233−12 861	(3.69 ± 0.08)e − 12
	600	10	242.7	317−73 009	(1.40 ± 0.03)e − 11
	600	30	243.0	314−114 302	(1.83 ± 0.02)e − 11
	600	45	242.5	308−150 218	(2.56 ± 0.04)e − 11
	600	60	242.6	297−99 435	(2.42 ± 0.04)e − 11
	600	90	242.8	285−155 472	(2.67 ± 0.05)e − 11
	600	120	242.3	314−170 355	(2.89 ± 0.05)e − 11
		Equation 2			
d_6-DMS	200	0	238.9	221−8074	(1.22 ± 0.02)e − 12
	200	0	239.8	235−6627	(1.28 ± 0.02)e − 12
	200	5	239.9	246−28 209	(5.40 ± 0.07)e − 12
	200	10	240.0	233−39 606	(7.62 ± 0.10)e − 12
	200	20	238.9	296−48 475	(9.26 ± 0.11)e − 12
	200	30	238.9	272−82 235	(1.11 ± 0.02)e − 11
	200	50	239.0	280−64 753	(1.19 ± 0.02)e − 11
	200	70	238.9	289−64 770	(1.30 ± 0.02)e − 11
	200	100	239.6	309−65 357	(1.27 ± 0.04)e − 11
	600	0	240.0	134−5955	(1.50 ± 0.02)e − 12
	600	4	240.0	195−30 551	(6.09 ± 0.08)e − 12
	600	10	237.5	251−71 466	(1.23 ± 0.04)e − 11
	600	15	238.0	235−85 235	(1.57 ± 0.04)e − 11
	600	30	237.5	235−119 539	(2.21 ± 0.05)e − 11
	600	45	237.5	252−156 380	(2.15 ± 0.08)e − 11
	600	60	237.5	180−150 107	(2.63 ± 0.07)e − 11
	600	90	240.0	293−139 521	(2.34 ± 0.06)e − 11
	600	120	237.5	180−80 440	(2.72 ± 0.06)e − 11

reaction with oxygen, k_s, was not directly measured, the fits of eq IX are sensitive to this parameter and allow the rate coefficient to be derived from the fit.

3. Theoretical Results. Geometry optimizations for the OH−DMS adduct, dimethylsulfide, and OH were completed at the MP2/6-31+G(2d,p) level of theory utilizing Gaussian 03.[43] The

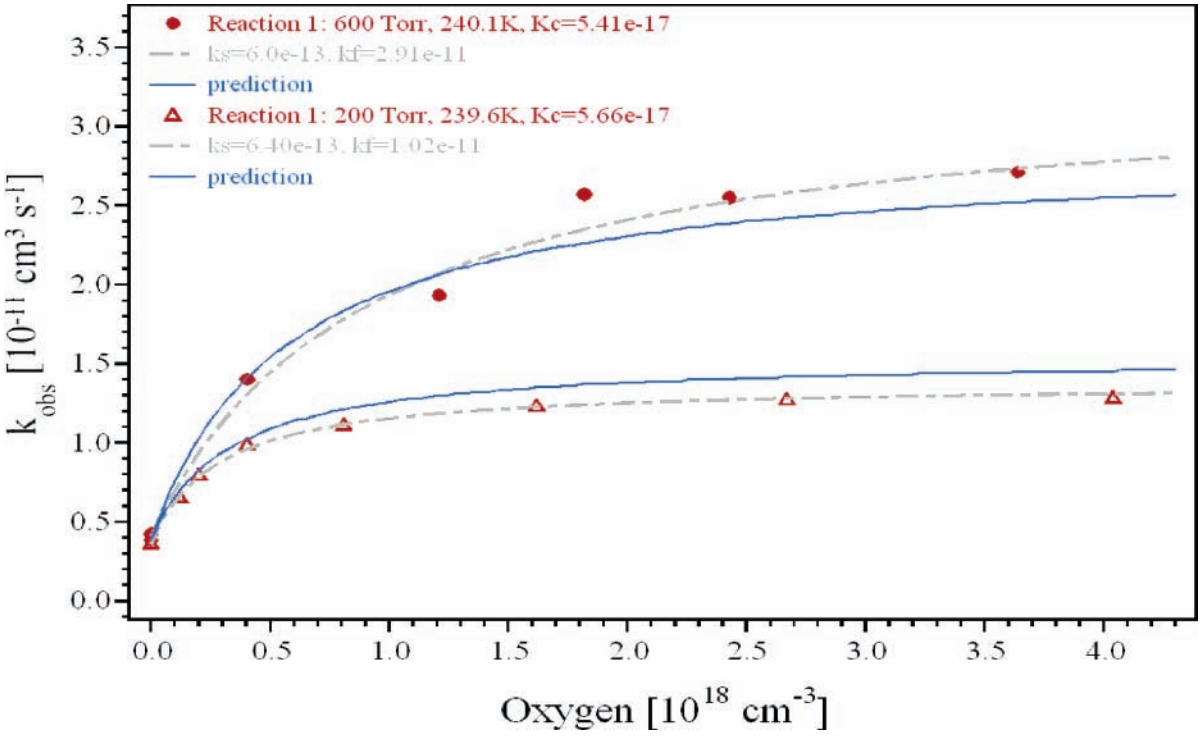

Figure 11. OH + h_6-DMS. Variation in the overall rate of oxidation, k_{obs} (k_{obs}= k_1), at both 200 Torr (triangles) and 600 Torr (circles) pressures and $T \sim 240$ K. Dashed lines are best fits of eq IX to the data when both k_s and k_f are free parameters. Solid lines are the ability of eq IX, using the expression outlined in Table 8, to reproduce oxygen-dependent data for eq 1. The *y*-intercept for both curves is k_a.

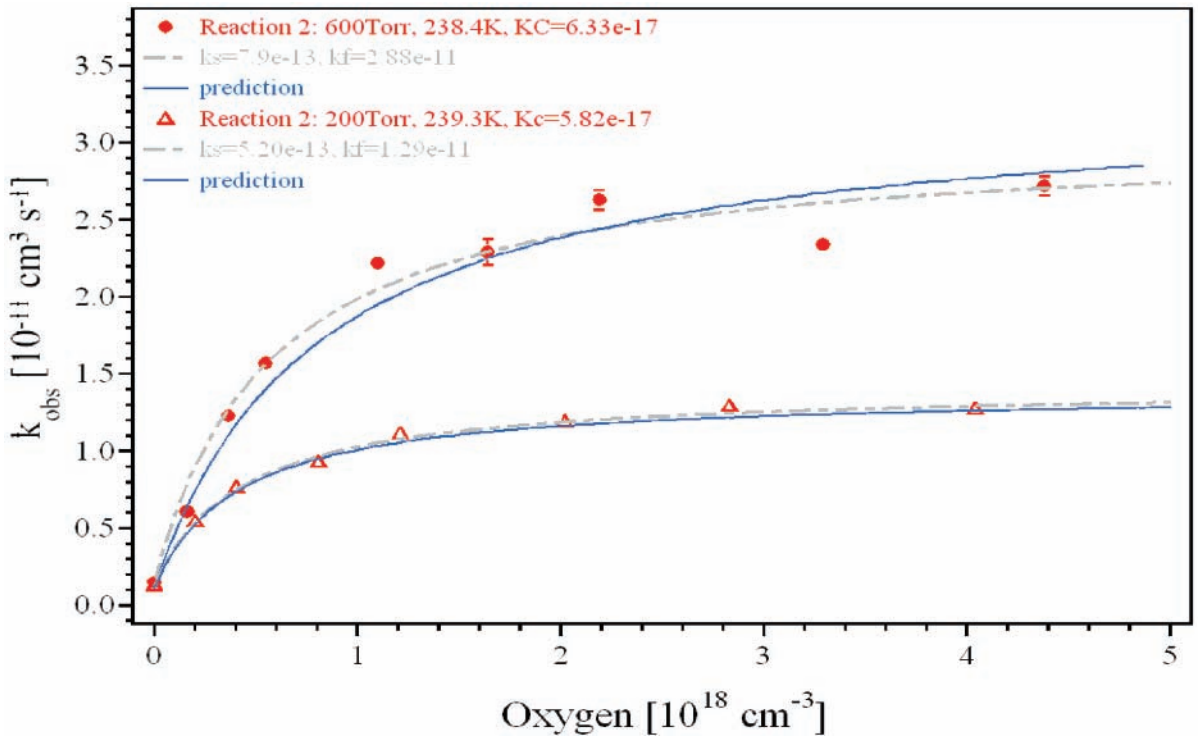

Figure 12. OH + d_6-DMS. Variation in the overall rate of oxidation, k_{obs} (k_{obs}= k_2), at both 200 Torr (triangles) and 600 Torr (circles) pressures and T $\sim$ 240 K. Dashed lines are best fits of eq IX to the data when both k_s and k_f are free parameters. Solid lines are the ability of eq IX, using the expression outlined in Table 8, to reproduce oxygen-dependent data for eq 2. The *y*-intercept for both curves is k_a.

optimized structure of OH−DMS is shown in Figure 13. Relevant bond lengths and angles are listed in Table 4 and are compared to prior results from the literature. While the structural values agree well with the work of McKee,[34] they are considerably different from the values reported by Turecek[37] and Gross et al.[44]

In a prior work, Gu and Turecek[36] performed ab-initio geometry optimizations on the dimethylhydroxylsulfanyl ion. Using the optimized geometries of the ion, they computed HF/6-31G* energies for the neutral molecule to demonstrate that the DMS−OH adduct was unstable with respect to dissociation to DMS and OH. McKee later demonstrated that minimally the

TABLE 3: Fits of Eq IX to Oxygen-Dependent Data[a]

sulfide	P (Torr)	T (K)	K_c van't Hoff relationship, this work, fixed	k_a (cm^3/molec-s) measured this work, fixed	k_s (cm^3/molec.-s), free	k_f (cm^3/molec.-s), free	k_f measured in equilibrium studies, this work
h_6-DMS	200	239.6	5.66e − 17	3.59e − 12	(6.40 ± 0.26)e − 13	(1.02 ± 0.03)e − 11	1.12e − 11
d_6-DMS	200	239.3	5.82e − 17	1.24e − 12	(5.17 ± 0.12)e − 13	(1.29 ± 0.19)e − 11	1.15e − 11
h_6-DMS	600	240.1	5.41e − 17	4.03e − 12	(6.00 ± 0.21)e − 13	(2.91 ± 0.05)e − 11	2.27e − 11 2.62e − 11
d_6-DMS	600	238.5	6.33e − 17	1.53e − 12	(7.97 ± 1.2)e − 13	(2.89 ± 0.16)e − 11	3.76e − 11

[a] Equilibrium constants and abstraction rates were fixed parameters. k_s and k_f were free parameters. Directly measured values of k_f from this work are listed for comparison.

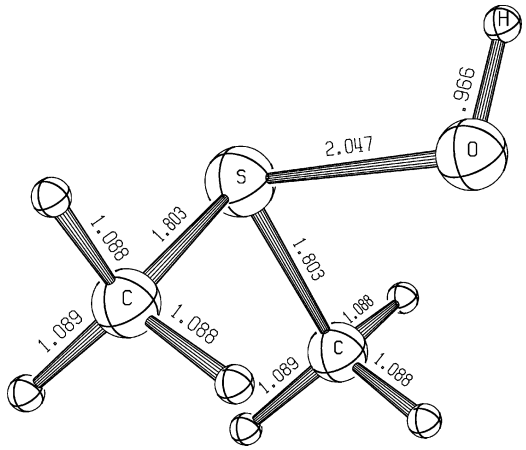

Figure 13. ORTEP[74] rendering of the optimized DMS−OH adduct geometry calculated at the MP2/6-31+G(2d,p) level of theory. Displayed bond lengths are in Å. Other relevant structural parameters are found in Table 4.

MP2/6-31+G(2d) level of theory was required to find a equilibrium structure with a minimum on the potential energy surface. Following this, Turecek[37] performed geometry optimizations on the DMS−OH adduct at the MP2/6-31+G(d) level, a smaller basis set than recommended by McKee, to conclude that the dimethylhydroxylsulfanyl radical does not represent a bound structure but rather a weak dipole−dipole complex.

The current calculations started minimally at the basis set and method suggested by McKee and added single polarization functions to the hydrogens, MP2/6-31+G(2d,p),[45−51] to examine the effect on the overall molecular geometry. In prior computational studies, optimizations included either diffuse and polarization functions on the heavy atoms only or a larger basis set which included polarization functions on all atoms but no diffuse functions. From the results (see Table 4), it is clear that inclusion of diffuse functions, which more accurately describe weakly bound states, into the molecular wavefunctions significantly reduces the S−O bond length when compared to methods that simply employed larger basis sets with no diffuse functions. It is also clear that the inclusion of polarization functions on the hydrogens had very little effect.

Vibrational frequencies for all species were calculated at the equilibrium geometry using the same level of theory as the geometry optimization. Vibrational frequencies were also calculated for CD_3SCD_3 and $CD_3S(OH)CD_3$ using the same geometries and electronic environment as their non-deuterated analogues. All of the calculated frequencies were positive indicating that the equilibrium structures were at a minimum on the potential energy surface. In addition, zero-point energies and 298 K enthalpy corrections were calculated at the MP2/6-31+G(2d,p) level of theory for the molecules studied. The results of these calculations are found in Table 5.

Utilizing the optimized MP2/6-31+G(2d,p) geometries, energies were improved by both increasing the level of correlation (utilizing MP4(SDTQ)[52] and QCISD(T))[53−55] and increasing the size of the basis set to 6-311+G(3df,2p).[56] The results of these calculations are found in Table 6.

Following the method of Ochterski,[57] binding energies, 0 K enthalpies, and 298 K enthalpies of reaction were computed for the reactions of CH_3SCH_3 and CD_3SCD_3 with OH using different basis sets and methods. The results of these calculations are found in Table 7. In a recent paper,[35] McKee used density functional theory (DFT) methods to compute the DMS−OH bond strength at −13.7 kcal/mol with a 298 K bond enthalpy of −11.9 kcal/mol. Our MP2 calculations at the MP2/6-311+G(3df,2p) level gave a DMS−OH bond strength of −11.16 kcal/mol and a 298 K bond enthalpy of −9.22 kcal/mol. DFT methods for these systems suffer from inverse symmetry breaking[58,59] and are known to overestimate the bond stabilities. Similarly, MP2, which is not a variational method and only minimally includes electron correlation, could overestimate the bond stability. In fact, this gives the closest value to our experimental determination but still underestimates the adduct stability. When the treatment of electron correlation was increased by using the MP4 methods, the bond strength was weakened by 1.77 kcal/mol. However, further increasing the amount of electron correlation by going from MP4 to QCISD(T) strengthened it by 0.23 kcal/mol to −9.62 kcal/mol.

On the basis of these computational results and the 2003 results from McKee,[35] the DMS−OH adduct is a stable species and the OH is chemically bound to the dimethylsulfide. The DFT results of McKee serve as an absolute lower bound for the DMS−OH bond strength and enthalpy. The QCISD(T) results presented here similarly serve as an upper bound for these quantities. The results of our calculations also indicate that the bond enthalpies for the deuterated reactions are slightly lower than the non-deuterated ones, although the difference is much smaller than the uncertainty associated with the precision of current experimental determinations. Finally, on the basis of the results of the electron correlation study, it is clear that a method incorporating a high level of electron correlation is needed to accurately treat the two center−three electron bond in the adduct.

Discussion

1. Pressure Dependence of k_f. Figures 5 and 6 show the pressure dependence of k_f, the rate coefficient for adduct formation for both isotopomers (k_{1b}, k_{2b}). The rate coefficients obtained from the analysis of the dependence of k_{obs} on oxygen concentration (solid triangles in Figure 5 and solid diamonds in Figure 6) are in good agreement with those obtained from fits to biexponential OH temporal profiles observed in N_2 at high DMS concentration (open triangles or open diamonds). It is clear that the precision of the values obtained from biexpo-

TABLE 4: MP2/6-31 + G(2d,p) Energies for the DMS−OH Adduct, DMS, and OH and the Relevant Structural Parameters for the Equilibrium DMS−OH Adduct Geometry

species	symmetry	state	absolute energy (hartrees)	structural parameter	this work	McKee[a,b] (1993)	Tureek[c,d] (1994)	Gross et al.[e,f] (2004)
$CH_3S(OH)CH_3$	C_s	$^2A'$	−552.789809604 32	S−O	2.047	2.047	2.579	3.292
				S−C	1.803	1.804	1.806	
				C−S−X	99.7	99.9	98.7	
				C−S−O	88.5	88.7	88.5	
				S−O−H	104.1	103.6	130.2	<45
CH_3SCH_3	C_{2v}	$^1A_1$	−477.20897284257					
OH	$C_{\infty v}$	$^2\Pi$	−75.565693601198					

[a] McKee, M. L. *J. Phys. Chem*. **1993**, *97*, 10971. [b] MP2/6-31+G(2d). [c] Turecek, F. *J. Phys. Chem*. **1994**, *98*, 3701. [d] MP2/6-31+G(d). [e] Gross, A.; Barnes, I.; S*o*rensen,R.; Kongsted, J.; Mikkelsen,K. *J. Phys. Chem.* **2004**, *108*, 8659. [f] MP2/6-311G(d,p).

TABLE 5: Unscaled Vibrational Frequencies (cm^{-1}), Zero-Point Energies (J/mol), and Enthalpy Corrections (J/mol) Calculated at Optimized MP2/6-31+G(2d,p) Geometry

species	frequencies	ZPE[a]	H_{298}[a]
CH_3SCH_3	191.9175, 197.6894, 266.0101, 712.8254, 766.6861, 934.5489, 973.0573, 1007.2219, 1068.4865, 1372.1134, 1396.9247, 1500.0054, 1510.5808, 1516.1708, 1525.0786, 3101.6115, 3106.4751, 3197.7638, 3206.2971, 3219.2555, 3220.317	190950.2	206469.5
CD_3SCD3	137.5606, 144.6469, 228.6334, 656.8785, 701.5985, 722.6606, 728.0157, 768.3762, 851.0106, 1051.5106, 1070.1069, 1083.6575, 1092.0427, 1098.9296, 1102.7837, 2221.6197, 2225.2503, 2372.3258, 2378.8949, 2385.6584, 2386.4036	142736.8	160003.3
$CH3(OH)CH_3$	60.8032, 160.9655, 181.6801, 245.271, 296.2876, 296.8488, 477.8806, 717.274, 773.998, 821.9266, 948.1633, 967.1137, 1000.9407, 1074.1857, 1363.3633, 1384.0642, 1485.7996, 1493.3574, 1498.812, 1507.1401, 3115.2701, 3117.8625, 3230.3804, 3232.9833, 3244.3461, 3244.9707, 3839.0677	223474.9	244681.0
$CD_3(OH)CD_3$	56.5063, 122.0328, 133.3377, 214.3089, 266.1815, 280.2379, 471.903, 660.8636, 704.602, 721.8705, 742.4408, 765.2574, 825.6296, 855.1534, 1048.9136, 1063.0836, 1075.1137, 1079.0938, 1084.1678, 1088.219, 2229.8624, 2231.7246, 2396.4959, 2397.3485, 2406.7211, 2406.8425, 3839.0617	175085.6	198141.4
OH	3817.2369	21443.9	30119.8

[a] No recommended value exists in the standard literature for the combination of MP2 with the 6-31+G(2d,p) basis set. 0.9392 is the recommended frequency scaling factor for MP2/6-31+G(d,p) calculations (CCCBDB vibrational frequency scaling factors, http://srdata.nist.gov/cccbdb/vsf.asp) and was used on the basis of the similarity to the basis set used for the calculations.

TABLE 6: Absolute Energies (Hartrees) Calculated at the Optimized MP2/6-31+G(2d,p) Geometry to Compare the Effect of Changing the Basis Set and f Electron Correlation

species	MP2/ 6-31+G(2d,p)	MP4(SDQ)/ 6-31+G(2d,p)	QCISD()/ 6-31+G(d,p)	MP2/ 6-311+G(3df,2p)	MP3(STQ)/ 6-311+G(3df,2p)	QCISDT)/ 6-311+G(3df,2p)
CH_3SCH_3	−477.20897284256	−477.26861398	−477.27009118	−477.32574508053	−477.39328116	−477.3937562 8
OH[a]	−75.565693601083	−75.582947999	−75.583971561	−75.617531723755	−75.636018118	−75.636853556
$CH_3S(OH)CH_3$	−552.78980960634	−552.8638262	−552.86724578	−552.96105822943	−553.04427048	−553.04593347

[a] $<S^2> < 0.76$ after spin annihilation.

TABLE 7: Comparison of Energies and Enthalpies (kcal/mol) of Reaction as a Function of Basis Set and Level of Electron Correleation Treatment for the Deuterated and Non-Deuterated Reactions[a]

		$CH_3SCH_3 + OH \rightarrow CH_3S(OH)CH_3$		$CD_3SCD_3 + OH \rightarrow CD_3S(OH)CD_3$	
method	ΔE_{rxn}[a b]	ΔH_{rxn}^{0K}	ΔH_{rxn}^{298K}	ΔH_{rxn}^{0K}	ΔH_{rxn}^{298K}
MP2-6-31+G(2d,p)	−9.5	−6.85	−7.57	−6.90	−7.59
MP4(SDTQ)/""	−7.7	−5.05	−5.76	−5.09	−5.78
QCISD(T)/""	−8.27	−5.62	−6.34	−5.67	−6.36
MP2/6-311+G(3df,2pd)		−8.51	−9.22	−8.55	−9.24
MP4(SDT)/""		−6.75	−7.46	−6.79	−7.48
QCISD(T)/""	−9.62	−6.97	−7.68	−7.01	−7.70

[a] In all cases, the zero-point energies and enthalpy corrections were computed at the MP2/6-31+G(2d,p) optimized geometry and level of theory. [b] Same for both reactions.

nential profiles is lower, and this reflects the difficulty of extracting rate coefficients from such temporal profiles when the two components of the decay have similar magnitudes. In this case, it also reflects the difficulty associated with the measurement of the initial, very rapid decay in the OH profile which corresponds to pseudo-first-order decay rates in excess of 4×10^6 s^{-1} at high pressures. The data suggest that there is a slight difference in the falloff behavior for eqs 1b and 2b, although the magnitude of this difference is obscured by the larger scatter in the d_6-DMS data set. The electronic structure calculations suggest that the two adducts (h_6-OHDMS or d_6-OHDMS) have similar binding energies and structures and that the high-pressure limits should be similar. To be prudent, both sets of data have been independently fit using the method of Troe.[60,61]

$$k = \frac{k_0[\mathrm{M}]}{1 + k_0[\mathrm{M}]/k_\infty} \cdot F_c \left[1 + \left(\frac{\log (k_0[\mathrm{M}]/k_\infty)}{N}\right)^2\right]^{-1} \qquad \text{(X)}$$

$$N = 0.75 - 1.27 * \log(F_c)$$

In accordance with theory, the fits have been forced through the origin even though no experimental points were taken at low pressures. They are noted in Figures 5 and 6 as nonexperi-

mental points. Constraining the fits with the physically realistic requirement that $F_c \leq 1$ gives values of k_{inf} which range from $\sim 1 \times 10^{-10}$ cm^3 molecule^{-1} s^{-1} for $F_c = 1$ to $\sim 3 \times 10^{-10}$ cm^3 molecule^{-1} s^{-1} for $F_c = 0.6$. Fits with $F_c = 1$ and $F_c = 0.6$ are virtually indistinguishable. To identify the values of k_{inf} and k_0 with physically realistic parameters, for example, to identify k_{inf} with the capture limit for formation of an energized OH−DMS adduct, an accurate value of F_c is required. The rate coefficients presented here are close to the low-pressure limit and show no indication of falloff behavior, so an attempt to extrapolate to an accurate value of k_{inf} is not possible. We can, however, compare the k_{inf} values with "proxy" values derived from vibrational deactivation studies. The use of vibrational deactivation as an experimental route to a proxy value for the limiting high-pressure rate, k_{inf}, has recently been reviewed by Smith.[62] The idea is that, in the absence of a potential barrier, the capture rate for a molecule such as OH should be largely independent of its vibration energy. As noted by Smith, for systems in which strong bonds are formed, the lifetime of the energized complex is likely to be such that, even without stabilization by a third body, randomization of the energy in the OH bond is highly likely. Redissociation will produce OH in a lower vibrational level because for a given energy there is a much higher volume of phase space associated with translations and rotations than with vibrations. Consequently, a direct measurement of the deactivation rate of vibrationally excited OH may offer a quantitative measurement of k_{inf}. In recent work, we measured rate coefficients for vibrational deactivation for OH ($v = 1-5$) by NO_2.[63] Our measured rate coefficients were independent of vibrational level and are in excellent agreement with a direct measure of k_{inf} for the OH + NO_2 recombination recently reported by Hippler et al.[64] The measured rate coefficients for deactivation of vibrationally excited OH by DMS were OH ($v = 1$): 2.55×10^{-11} cm^3 molecule^{-1} s^{-1} and OH ($v = 2$): 5.34×10^{-11} cm^3 molecule^{-1} s^{-1}. The observation that the deactivation rate coefficients for $v = 1$ and 2 are significantly different is consistent with the weakly bound nature of OH−DMS and suggests that the lifetime of the adduct is very short. Consequently, a statistical redistribution of energy is not possible before adduct redissociation, and hence, the OH retains some of its initial vibrational excitation. These results should give a lower limit to the rate coefficient for the high-pressure limit for adduct formation suggesting that it must be greater than 5.34×10^{-11} cm^3 molecule^{-1} s^{-1}. In addition, observations in this laboratory on adduct formation in other alkylsulfides[65] are consistent with a high-pressure limit of $\geq 1 \times 10^{-10}$ cm^3 molecule^{-1} s^{-1}. In the absence of any other data on the high-pressure limit, we have fit the data as a simple parametrization for both isotopomers with a value of $F_c = 1$, which treats adduct formation as being well described by the simple Lindemann mechanism. This is not realistic physically, and the values of k_0 and k_{inf} which are obtained are simply fitting parameters rather than rate coefficients which can be compared with experimental or theoretical values. As Figures 5 and 6 show, the experimental observations are well described by this approach and a simple parametrization results. The values of k_0 and k_{inf} are

$$k_{1b,0} = (1.78 \pm 0.23) \times 10^{-30} \text{ cm}^6 \text{ molecule}^{-2} \text{ s}^{-1}$$

$$k_{1b,\infty} = (5.82 \pm 1.33) \times 10^{-11} \text{ cm}^3 \text{ molecule}^{-1} \text{ s}^{-1}$$

$$k_{2b,0} = (1.72 \pm 0.37) \times 10^{-30} \text{ cm}^6 \text{ molecule}^{-2} \text{ s}^{-1}$$

$$k_{2b,\infty} = (1.33 \pm 1.18) \times 10^{-10} \text{ cm}^3 \text{ molecule}^{-1} \text{ s}^{-1}$$

The error limits on k_{inf} are the 2σ error of the fit when both k_0 and k_{inf} are free parameters. The errors are large because of the scatter in the data and because of the extrapolation made on this data set where we are still in the falloff region. Hence, the difference in the values for $k_{\infty(1b)}$ and $k_{\infty(2b)}$, although large, is within the error bars.

2. Adduct Reaction with O_2. The values of k_s determined from fits to the oxygen-dependent data in this work range from 5.17×10^{-13} cm^3 molecule^{-1} s^{-1} to 7.97×10^{-13} cm^3 molecule^{-1} s^{-1} and give an average value of $6.3 \pm 1.2 \times 10^{-13}$ cm^3 molecule^{-1} s^{-1} (Table 3) in good agreement with the rate coefficient obtained in our prior work at 100 Torr where $k_s = 8 \pm 3 \times 10^{-13}$ cm^3 molecule^{-1} s^{-1} [18] and in reasonable agreement with the value obtained by Barone et al., $1.00 \pm 0.33 \times 10^{-12}$ cm^3 molecule^{-1} s^{-1}, at 100 Torr in both He and N_2. It suggests that k_s is independent of pressure and shows no isotopic dependence and little temperature dependence over this range. Previous mechanistic studies have suggested that reaction of the adduct with O_2 produces HO_2 and DMSO.

$$CH_3S(OH)CH_3 + O_2 \rightarrow CH_3S(O)CH_3 + HO_2 \quad (3a)$$

However, if eqs 3 and 4 proceeded via a channel which produces OH,

$$CH_3S(OH)CH_3 + O_2 \rightarrow CH_3S(O_2)CH_3 + OH \quad (3b)$$

$$CD_3S(OH)CD_3 + O_2 \rightarrow CD_3S(O_2)CH_3 + OH \quad (4b)$$

then the values of k_{obs} in the oxygen-dependent studies would underestimate the true value of k_{obs} because the contribution of eq 3b or 4b would not be measured in our experiments. As we have discussed previously,[11,41] if this were the case, we would expect the values of k_f derived from equilibrium measurements to be systematically higher than values derived from oxygen-dependent studies at the same pressure. In this work, equilibration (k_{1b}/k_{-1b} or k_{2b}/k_{-2b}) was directly measured. Second, the oxygen dependence of the effective rate coefficient was measured for all sulfides at two pressures (200 Torr and 600 Torr) and at 240 K. Values of k_f derived from equilibration measurements are in good agreement with those derived from the oxygen dependence of the effective rate coefficient indicating that a reaction channel regenerating OH is minor at 240 K. Unless the branching ratio for eqs 3 and 4 has a significant temperature dependence which seems unlikely, OH regeneration cannot explain differences between early direct studies[18] and chamber measurements.[19] Use of the independently determined values of K_c to fit the oxygen-dependent data is a robust diagnostic for correct mechanistic interpretation. The consistency between the data sets suggests that the two-channel mechanism is able to explain the measurements and that OH regeneration is insignificant.

3. Predictive Expression. As noted above, for many years the accepted effective rate coefficient for eq 1 and the branching ratio between the addition and abstraction channels has been taken from the expression developed by Hynes et al. in 1986. The current IUPAC recommendation is a parametrization based on our 600 Torr oxygen-dependent data,[13] and it parametrizes the overall rate of oxidation solely in terms of O_2. It does not take into account pressure dependence associated with k_{1b}. In both cases, these parametrizations are not based on direct

TABLE 8: Parameters Used in Eq IX to Generate a Predictive Expression of k_1 and k_2 at Various Pressures and at $T \sim 240$ K

term	parameters in eq IX	source
k_{1a}	(7.68e − 12)exp(−167/T)	Arrhenius fit of h_6-DMS data: this work
k_{2a}	(1.591e − 11)exp(−630/T)	Arrhenius fit of d_6-DMS data: this work
k_{1b}	eq X: $k_0 = 1.78e - 30$, $k_\omega = 5.82e - 11$, $F = 1.0$	Troe fit of h_6-DMS data: this work
k_{2b}	eq X: $k_0 = 1.72e - 30$, $k_\omega = 1.33e - 10$, $F = 1.0$	Troe fit of d_6-DMS data: this work
K_c	T dependent	van't Hoff line: Figure 8
k_{-1b}	k_{1b}/K_c	
k_{-2b}	k_{2b}/K_c	
k_3	$(6.3 \pm 1.7) \times 10^{-13}$ cm^3/molec-s	this work
k_4	$(6.3 \pm 1.7) \times 10^{-13}$ cm^3/molec-s	this work

determinations of the elementary rate coefficients and are only appropriate for 1 atm of air. The data set presented here allows us to present a predictive expression on the basis of measured elementary rates that gives the effective rate coefficient and branching ratio at low temperature for any atmospheric pressure and oxygen concentration. The expression for calculating k_{obs} was obtained by substituting expressions for the elementary rate coefficients into eq IX. These parameters and their sources are listed in Table 8 and allow calculation of the effective rate at any appropriate pressure and temperature. Slight differences were observed in d_6-DMS and h_6-DMS data sets, and while only the parameters for calculation of eq 1 are necessary for atmospheric modeling, we show the parameters for calculation of eq 2 for comparison with our d_6-DMS data set in Figure 12.

Using the values in Table 8 and eq IX, k_{obs} was calculated as a function of oxygen partial pressure at 240 K and total pressures of 200 and 600 Torr to give the solid lines shown in Figure 11 for h_6-DMS and in Figure 12 for d_6-DMS. The expression does a reasonable job of reproducing both the 200 and 600 Torr data sets at $T \sim 240$ K, using the temperature- and pressure-independent value for $k_s = 6.3 \pm 1.2 \times 10^{-13}$ cm^3 molecule^{-1} s^{-1} (the average of values determined in this work) and K_c values determined in this work. This expression underpredicts the maximum values observed for eq 1 at 600 Torr and slightly overpredicts the values at 200 Torr. In both cases, the discrepancy is roughly 10%. The expression is able to reproduce rate coefficients obtained in this laboratory at 240 K (to within 15%) and at 261 K (to within 40%),[11,18,] h_6-DMS data of Barone et al. at 247 K and 100 Torr of N_2,[14] and recent data from Albu et al. at 760 Torr over the range 270−250 K. This expression also reproduces the rate enhancements in d_6-DMS rate coefficients seen in the 1995 work of Hynes et al. and the Barone et al. work. We believe that it can be used between 260 and 220 K at pressures up to 760 Torr, rendering eq IX appropriate for various regions of the lower, polar troposphere as well as portions of the mid and upper troposphere where DMS can be present because of convective pumping.[66] We are in the process of developing an expression appropriate for the full temperature range of the troposphere and the pressure range 50−760 Torr.

4. Atmospheric Implications. In previous work,[13] we demonstrated that the effective rate coefficient for eq 1 was significantly faster at low temperatures than that derived from the expression published in the 1986 work of Hynes et al. As a consequence, the branching ratio between the addition and abstraction channels is significantly larger than predicted by the previous expression. In this work, we have shown that the elementary rates for adduct formation and decomposition and the rate of reaction of the adduct with O_2 are entirely consistent with these faster rates. A recently published competitive rate study of eq 1 at temperatures between 300 and 250 K is also consistent with these observations.[16]

Temperature dependence in the abstraction/addition branching ratio is often used to interpret the distribution of methansulfonate to non-sea-salt-sulfate ratio as measured in the marine boundary layer and in ice cores,[33,67−71] however, these interpretations have had limited success. Ravishankara and co-workers have suggested that the initial branching step cannot explain the observed temperature dependence of such things as the methanesulfonate: non-sea-salt-sulfate ratio in aerosols.[15,72,73] They have suggested that the measured bond strength for the DMS·OH adduct is not compatible with the branching ratio between abstraction and addition that is required to explain the large increases in the MSA/sulfate ratio.[15] The complexity and uncertainties in the DMS oxidation mechanism are such that inferences on the relationship between field observables and the elementary steps in the mechanism should be made with caution. Our work shows that the temperature dependence of the branching ratio is certainly not limited by the OH−DMS adduct bond strength but rather by the magnitude of the forward addition rate. Furthermore, the revised temperature dependence of the branching ratio between abstraction and addition is large enough to encompass most of the changes seen in the temperature dependence of field data such as the MSA:non-sea-salt ratio.[33,68] Clearly, this does not prove that the branching between addition and abstraction is actually responsible for these changes, but it does not preclude the initial steps influencing final product distributions under certain conditions.

Conclusions

The OH initiated oxidation of DMS proceeds via a complex mechanism involving reactions with molecular oxygen. As a consequence, the effective rate coefficient for the reaction shows a complex dependence on temperature and pressure. In spite of a multitude of experimental studies, the number of direct studies under realistic atmospheric conditions is very limited. For many years, the effective rate coefficients and branching ratios reported by Hynes et al. in 1986 were recommended for atmospheric modeling purposes. In this work, we demonstrate that, at low temperatures, the 1986 work underestimates both the effective rate coefficients and the branching ratio between the addition and abstraction channels. We measure both the effective rate coefficients as a function of pressure and gas composition at 240 K and in addition we measure the elementary rate coefficients for adduct formation and reaction with O_2. We show that the measured elementary rate coefficients are consistent with the observed effective rate coefficients. This suggests that our assumed two-channel mechanism is correct and allows us to develop an expression for the effective rate coefficient on the basis of that mechanism. The expression accurately captures the rates of eqs 1 and 2 at any total pressure up to 1 atm for any partial pressure of O_2 at temperatures between 260 and 220 K. In addition, electronic structure calculations have been used to calculate the structure of the OH−DMS adduct and its deuterated isotopomer. We find similar bound structures for both isotopomers. The calculated reaction enthalpies for adduct formation are a little lower than the experimentally determined values.

Specifically, temporal profiles for the formation of the h_6-OHDMS and d_6-OHDMS adducts have been measured over a range of pressures approaching 1 atm and at a temperature of ~240 K. Analysis of these profiles has given the rate coefficients for adduct formation and adduct decomposition and hence the equilibrium constants. Van't Hoff analysis gives an adduct bond strength in good agreement with previously reported values. The rate coefficients for the formation of the adduct isotopomers showed slight differences in their falloff behavior. Rate coefficients were obtained for the effective rate coefficients of eqs 1 and 2 as a function of oxygen concentration at 200 and 600 Torr in the region of 240 K. Rate coefficients for adduct formation obtained from analysis of oxygen-dependent data were in good agreement with directly measured values demonstrating internal consistency of the two-channel reaction mechanism and indicating that OH regeneration via channel 3b or 4b is insignificant. Directly determined equilibrium constants were used successfully to fit oxygen-dependent data, demonstrating sound mechanistic interpretation. The rate coefficient for the reaction of the adducts with O_2 (k_3, k_4) shows no isotopic or pressure dependence over the range 200−600 Torr.

Our recent work on the oxygen dependence of the effective rate coefficients for eqs 1 and 2 at 600 Torr total pressure and at low temperature[13] showed that the 1986 expression of Hynes et al.[18] underestimated both the overall rate of oxidation as well as the branching ratio at low temperatures by a factor of 2. The addition of our 200 Torr data over the same temperature range together with the equilibration data presented here provides a consistent picture of the OH initiated oxidation mechanism at low temperature and allows us to formulate an expression which can be used to calculate the effective rate coefficient for eq 1 at any pressure and oxygen concentration between 220 K and 260 K. The estimated error is ±40%, with the largest error being at the extremes of this temperature range. This data set is the first to include direct observation of equilibration over a range of pressures in N_2 approaching 1 atm, and the predictive expression developed in this work resolves discrepancies in the kinetic database and rectifies errors in the widely used expression from the 1986 work of Hynes et al. We are currently working on an expression appropriate for a larger temperature range.

Acknowledgment. This work was funded by the Office of Naval Research through grant N000149910032.

References and Notes

(1) Vairavamurthy, A.; Andreae, M. O.; Iverson, M. O. *Limnol. Oceanogr.* **1985**, *30*, 59.

(2) Watts, S. F. *Atmos. Environ.* **2000**, *34*, 761.

(3) Bates, T. S.; Calhoun, J. A.; Quinn, P. K. *J. Geophys. Res.* **1992a**, *97*, 9859.

(4) Seinfeld, J. N.; Pandis, S. N. *Atmospheric Chemistry and Physics*; Wiley-Interscience: New York, 1998.

(5) Pandis, S. N.; Russell, L. M.; Seinfeld, J. H. *J. Geophys. Res.* **1994**, *99*, 16945.

(6) Charlson, R. J.; Lovelock, J. E.; Andreae, M. O.; Warren, S. G. *Nature* **1987**, *326*, 655.

(7) Gabric, A. J.; Cropp, R.; Hirst, T.; Marchant, H. *Tellus B* **2003**, *55*, 966.

(8) Gabric, A. J.; Whetton, P. H.; Boers, R.; Ayers, G. P. *Tellus* **1998**, *50*, 388.

(9) Gabric, A. J.; Whetton, P. H.; Cropp, R. *Tellus* **2001**, *53B*, 273.

(10) Tyndall, G.; Ravishankara, A. R. *Int. J. Chem. Kinet.* **1991**, *23*, 483.

(11) Hynes, A. J.; Stoker, R. B.; Pounds, A. J.; McKay, T.; Bradshaw, J. D.; Nichovich, J. M.; Wine, P. H. *J. Phys. Chem.* **1995**, *99*, 16967.

(12) Silvente, E.; Richter, R. C.; Hynes, A. J. *J. Chem. Soc., Faraday Trans.* **1997**, *93*, 2821.

(13) Williams, M. B.; Campuzano-Jost, P.; Bauer, D.; Hynes, A. J. *Chem. Phys. Lett.* **2001**, *344*, 61.

(14) Barone, S. B.; Turnipseed, A. A.; Ravishankara, A. R. *J. Phys. Chem.* **1996**, *100*, 14694.

(15) Turnipseed, A. A.; Barone, S. B.; Ravishankara, A. R. *J. Phys. Chem.* **1996**, *100*, 14703.

(16) Albu, M.; Barnes, I.; Becker, K. H.; Patroescu-Klotz, I.; Mocanu, R.; Benter, T. *Phys. Chem. Chem. Phys.* **2005**, *8*, 728.

(17) Barnes, I.; Hjorth, J.; Mihalopoulos, N. *Chem. Rev.* **2006**, *106*, 940.

(18) Hynes, A. J.; Wine, P. H.; Semmes, D. H. *J. Phys. Chem.* **1986**, *90*, 4148.

(19) Barnes, I.; Bastian, V.; Becker, K. H. *Int. J. Chem. Kinet.* **1988**, *20*, 415.

(20) Wallington, T. J.; Atkinson, R.; Tuazon, E. C.; Aschmann, S. M. *Int. J. Chem. Kinet.* **1986**, *18*, 837.

(21) Berresheim, H.; Wine, P. H.; Davis, D. D. Sulfur in the Atmosphere. In *Composition, Chemistry and Climate of the Atmosphere*; Singh, H. B., Ed.; Van Nostrand Reinhold: New York, 1995; p 251.

(22) Atkinson, R.; Baulch, D. L.; Cox, R. A.; Crowley, J. N.; Hampson, R. F. Summary of Evaluated Kinetic and Photochemical Data for Atmospheric Chemistry (web version); IUPAC Subcommittee on Gas Kinetic Data Evaluation for Atmospheric Chemistry, 2002. www.iupac-kinetic.ch.cam.ac.uk.

(23) Atkinson, R.; Baulch, D. L.; Cox, R. A.; Hampson, R. F., Jr.; Kerr, J. A.; Troe, J. *J. Phys. Chem. Ref. Data* **1992**, *21*, 1125.

(24) Sander, S. P.; Kurylo, M. J.; Orkin, V. L.; Golden, D. M.; Huie, R. E.; Finlayson-Pitts, B. J.; Molina, M. J.; Friedl, R. R.; Ravishankara, A. R.; Moortgart, G. K. *Chemical Kinetics and Photochemical Data for Use in Atmospheric Studies*; JPL Data Evaluation #14, 02-25 ed.; NASA: Jet Propulsion Laboratory, Pasadena, California, 2003.

(25) Williams, M. B.; Campuzano-Jost, P.; Bauer, D.; Hynes, A. J. Direct observations of the OHDMS adduct -reevaluation of the rate and branching ratio. Presented at American Geophysical Union Annual Meeting, San Franciso, CA, 1999.

(26) Williams, M. B.; Campuzano-Jost, P.; Bauer, D.; Hynes, A. J. Kinetic and mechanistic studies of the OH-initiated oxidation of dimethylsulfide at low temperature - A reevaluation of the rate and branching ratio. Presented at Fifth International Conference on Chemical Kinetics, Gaithersburg, MD, 2001.

(27) Hynes, A. J.; Rosendahl, A. R.; Nien, C. J. OH + DMS: Observations in the presence of Nitric Acid. Unpublished work, 2003.

(28) Hynes, A. J.; Stickel, R. E.; Pounds, A. J.; Zhao, Z.; McKay, T.; Bradshaw, J. D.; Nicovich, J. M.; Wine, P. H. Mechanistic Studies of the OH-Initiated Oxidation of Dimethylsulfide. In *Dimethylsulfide: Oceans, Atmosphere and Climate*; Restelli, G., Angelletti, G., Eds.; Kluwer Academic Publishers: Boston, MA, 1993; p 211.

(29) Arsene, C.; Barnes, I.; Becker, K. H. *Phys. Chem. Chem. Phys.* **1999**, *1*, 5463.

(30) Arsene, C.; Barnes, I.; Becker, K. H.; Mocanu, R. *Atmos. Environ.* **2001**, *35*, 3769.

(31) Patroescu, I. V.; Barnes, I.; Becker, K. H.; Mihalopoulos, N. *Atmos. Environ.* **1999**, *33*, 13.

(32) Arsene, C.; Barnes, I.; Becker, K. H.; Schneider, W. F.; Wallington, T. J.; Mihalopoulos, N.; Patroescu, I. *Environ. Sci. Technol.* **2002**, *36*, 5155.

(33) Yvon, S. A.; Saltzman, E. S. *J. Geophys. Res. Atmos.* **1996**, *101*, 6911.

(34) McKee, M. L. *J. Phys. Chem.* **1993**, *87*, 10971.

(35) McKee, M. L. *J. Phys. Chem.* A **2003**, *107*, 6825.

(36) Gu, M.; Turecek, F. *J. Am. Chem. Soc.* **1992**, *114*, 7146.

(37) Turecek, F. *J. Phys. Chem.* **1994**, *98*, 3701.

(38) Turecek, F. *J. Phys. Chem.* **1994**, *98*, 3701.

(39) Campuzano-Jost, P.; Williams, M. B.; D'Ottone, L.; Hynes, A. J. *Geophys. Res. Lett.* **2000**, *27*, 693.

(40) D'Ottone, L.; Campuzano-Jost, P.; Bauer, D.; Hynes, A. J. *J. Phys. Chem. A* **2001**, *105*, 10538.

(41) Hynes, A. J. Reaction Mechanisms in Atmospheric Chemistry: Detailed Kinetic and Mechansitic Studies of Hydroxyl Radical Reactions Under Atmospheric Conditions. In *Advances in Spectroscopy: Spectroscopy in Environmental Science*; Clark, R. J. H., Hester, R. E., Eds.; John Wiley & Sons: New York, 1995; Vol. 24, p 309.

(42) Williams, M. B.; Campuzano-Jost, P.; Riemer, D. D.; Tatum, C.; Hynes, A. J. *J. Photochem. Photobiol., A* **2004**, doi: 10.1016/j.photochem.2004.09.008.

(43) Frisch, M. J.; Trucks, G. W.; Schlegel, H. B.; Scuseria, G. E.; Robb, M. A.; Cheeseman, J. R.; Montgomery, J. A., Jr.; Vreven, T.; Kudin, K. N.; Burant, J. C.; Millam, J. M.; Iyengar, S. S.; Tomasi, J.; Barone, V.; Mennucci, B.; Cossi, M.; Scalmani, G.; Rega, N.; Petersson, G. A.; Nakatsuji, H.; Hada, M.; Ehara, M.; Toyota, K.; Fukuda, R.; Hasegawa, J.; Ishida, M.; Nakajima, T.; Honda, Y.; Kitao, O.; Nakai, H.; Klene, M.; Li, X.; Knox, J. E.; Hratchian, H. P.; Cross, J. B.; Bakken, V.; Adamo, C.; Jaramillo, J.; Gomperts, R.; Stratmann, R. E.; Yazyev, O.; Austin, A. J.; Cammi, R.; Pomelli, C.; Ochterski, J. W.; Ayala, P. Y.; Morokuma, K.; Voth, G. A.; Salvador, P.; Dannenberg, J. J.; Zakrzewski, V. G.; Dapprich,

S.; Daniels, A. D.; Strain, M. C.; Farkas, O.; Malick, D. K.; Rabuck, A. D.; Raghavachari, K.; Foresman, J. B.; Ortiz, J. V.; Cui, Q.; Baboul, A. G.; Clifford, S.; Cioslowski, J.; Stefanov, B. B.; Liu, G.; Liashenko, A.; Piskorz, P.; Komaromi, I.; Martin, R. L.; Fox, D. J.; Keith, T.; Al-Laham, M. A.; Peng, C. Y.; Nanayakkara, A.; Challacombe, M.; Gill, P. M. W.; Johnson, B.; Chen, W.; Wong, M. W.; Gonzalez, C.; Pople, J. A. *Gaussian 03*, revision C.02; Gaussian, Inc.: Wallingford, CT, 2004.

(44) Gross, A.; Barnes, I.; Sorensen, R. M.; Kongsted, J.; Mikkelsen, K. V. *J. Phys. Chem. A* **2004**, *108*, 8659.

(45) Frisch, M.; Head-Gordon, M.; Pople, J. *Chem. Phys. Lett*. **1990**, *166*, 275.

(46) Frisch, M.; Head-Gordon, M.; Pople, J. *Chem. Phys. Lett*. **1990**, *166*, 281.

(47) Head-Gordon, M.; Head-Gordon, T. *Chem. Phys. Lett*. **1994**, *220*, 122.

(48) Head-Gordon, M.; Pople, J.; Frisch, M. *Chem. Phys. Lett*. **1988**, *153*, 503.

(49) Frisch, M.; Pople, J.; Binkley, J. S. *J. Chem. Phys.* **1984**, *80*, 3265.

(50) Clark, T.; Chandrasekhar, J.; Spitznagel, G. W.; Schleyer, P. V. *J. Comput. Chem.* **1983**, *4*, 294.

(51) Ditchfield, R.; Hehre, W. J.; Pople, J. *J. Chem. Phys.* **1971**, *54*, 724.

(52) Krishnan, R.; Pople, J. *Int. J. Quantum Chem.* **1978**, *14*, 91.

(53) Pople, J.; Head-Gordon, M.; Raghavachari, K. *J. Chem. Phys.* **1987**, *87*, 5968.

(54) Gauss, J.; Cremer, D. *Chem. Phys. Lett*. **1988**, *150*, 280.

(55) Salter, E. A.; Trucks, G. W.; Bartlett, R. J. *J. Chem. Phys.* **1989**, *90*, 1752.

(56) Raghavachari, K.; Trucks, G. W. *J. Chem. Phys.* **1989**, *91*, 1062.

(57) Ochterski, J. Thermochemistry in Gaussian; Gaussian.com, Ed.; Wellingford, CT, 2000.

(58) Bally, T.; Sastry, G. N. *J. Phys. Chem. A* **1997**, *101*, 7923.

(59) Grafenstein, J.; Kraka, E.; Cremer, D. *J. Chem. Phys.* **2004**, *120*, 524.

(60) Troe, J. *J. Chem. Phys.* **1977**, *66*, 4745.

(61) Troe, J. *J. Phys. Chem.* **1979**, *83*, 114.

(62) Smith, I. W. M. *J. Chem. Soc., Faraday Trans.* **1997**, *93*, 3741.

(63) D'Ottone, L.; Bauer, D.; Campuzano-Jost, P.; Fardy, M.; Hynes, A. J. *Faraday Discuss.* **2005**, *130*, 111.

(64) Hippler, H.; Krasteva, N.; Nasterlack, S.; Striebel, F. *J. Phys. Chem. A* **2006**, *110*, 6781.

(65) Williams, M. B.; Campuzano-Jost, P.; Bauer, D.; Hynes, A. J. OH initiated oxidation of reduced sulfides. Presented at Informal conference on photochemistry, Miami, FL, 2002.

(66) Clarke, A. D.; Varner, J. L.; Eisele, F.; Mauldin, R. L.; Tanner, D.; Litchy, M. *J. Geophys. Res. Atmos.* **1998**, *103*, 16397.

(67) De Bruyn, W. J.; Bates, T. S.; Cainey, J. M.; Saltzman, E. S. *J. Geophys. Res. Atmos.* **1998**, *103*, 16703.

(68) De Bruyn, W. J.; Harvey, M.; Cainey, J.; Saltzman, E. S. *J. Atmos. Chem.* **2002**, *41*, 189.

(69) Legrand, M.; Feniet-Saigne, C.; Saltzman, E. S.; Germain, C.; Barkov, N. I.; Petrov, V. N. *Nature* **1991**, *350*, 144.

(70) Petit, J. R.; Basile, I.; Leruyuet, A.; Raynaud, D.; Lorius, C.; Jouzel, J.; Stievenard, M.; Lipenkov, V. Y.; Barkov, N. I.; Kudryashov, B. B.; Davis, M.; Saltzman, E. S.; Kotlyakov, V. *Nature* **1997**, *387*, 359.

(71) Saltzman, E. S.; Whung, P. Y.; Mayewski, P. A. *J. Geophys. Res.* **1997**, *102*, 26.

(72) Barone, S. B.; Turnipseed, A. A.; Ravishankara, A. R. *Faraday Discuss.* **1995**, *100*, 39.

(73) Ravishankara, A. R.; Rudich, Y.; Talukdar, R.; Barone, S. B.; LeBras, G.; Fish, J. D.; Ayres, G. P.; Cox, R. A. *Philos. Trans. R. Soc. London, Ser. B* **1997**, *352*, 171.

(74) Burnett, M. N.; Johnson, C. K. ORTEP-III: Oak Ridge Thermal Ellipsoid Plot Program for Crystal Structure Illustrations, 1996.